6-3-2004

Detached Eddy Simulation Analysis of Pak-B Low Pressure Turbine Blade

Kyle Malone

DETACHED EDDY SIMULATION ANALYSIS OF PAK-B LOW PRESSURE TURBINE BLADE

THESIS

Kyle P. Malone, Ensign, USNR

AFIT/GAE/ENY/04J-06

DEPARTMENT OF THE AIR FORCE
AIR UNIVERSITY

AIR FORCE INSTITUTE OF TECHNOLOGY

Wright-Patterson Air Force Base, Ohio

The views expressed in this thesis are those of the author and do not reflect the official policy or position of the United States Navy, United States Air Force, Department of Defense, or the United States Government.

AFIT/GAE/ENY/04J-06

DETACHED EDDY SIMULATION ANALYSIS OF PAK-B LOW PRESSURE TURBINE BLADE

THESIS

Presented to the Faculty

Department of Aeronautics and Astronautics

Graduate School of Engineering and Management

Air Force Institute of Technology

Air University

Air Education and Training Command

In Partial Fulfillment of the Requirements for the

Degree of Master of Science in Aeronautical Engineering

Kyle P. Malone, BS

Ensign, USNR

June 2004

AFIT/GAE/ENY/04J-06

DETACHED EDDY SIMULATION ANALYSIS OF PAK-B LOW PRESSURE TURBINE BLADE

Kyle P. Malone, BS
Ensign, USNR

Approved:

//signed//	03 June 2004
Dr. Paul King (Chairman)	date
//signed//	03 June 2004
Lt Col Raymond Maple (Member)	date
//signed//	03 June 2004
Dr. Mark Reeder (Member)	date

Abstract

Two cases were computationally investigated using the detached eddy simulation (DES) turbulence model: an unmodified Pak-B blade and a Pak-B blade with a dimple located at 65% of axial chord. Both cases were created so that they simulated an infinite span with an infinite number of dimples. The cases were run for an inlet Reynolds number of 25,000. The computed results were used to resolve the location of separation and reattachment, visualize the streamlines for the dimpled case, build velocity magnitude contour and vector plots, and map the thickness of the boundary layer. The results were then compared to previous computational and experimental studies in order to validate the detached eddy simulation model for future research into the effect of dimples on low pressure turbine flow fields. For the unmodified blade, the performance of the DES model compared favorably to other available viscous and turbulence models. For the dimpled blade, preliminary results also indicate favorable results although further development of the flow field is necessary to verify this. Based on these results, future researchers studying dimples on turbine blades should strongly consider using the DES turbulence model.

Acknowledgments

First, I would like to thank Dr. Paul King, my thesis advisor. From the beginning, he has helped to shape and direct the course of this research.

This project has been made possible by a grant of computing time from the DOD High Performance Computing Modernization Program at ASC/MSRC. In particular, I would like to thank Dr. Hugh Thornburgh from the ASC/MSRC staff. He has worked hard to develop the computational models and work through the numerous problems that arose in the course of this project. Also, I would like to thank the computer support personnel who set up my account and taught me how to use the MSRC network with which I was unfamiliar.

At AFIT, I would particularly like to thank LtCol Maple who taught me the basics of CFD and also helped to direct the course of this project. Also, 2Lt John Casey, whose work I built upon, was instrumental in getting my research started and in teaching me the basics of Fieldview®.

Finally, and most importantly, I would like to thank my family and friends who supported me throughout this process. I could not have completed this project without their contributions.

Kyle P. Malone

Table of Contents

List of Figures

List of Symbols

Symbol	Definition
C_D	drag coefficient
C_{DES}	DES model constant
C_L	lift coefficient
c_p	specific heat at constant pressure [J/kg-K]
D	diameter [m]
$\tilde{d}$	distance parameter modified for DES turbulence model [m]
dP	differential change in pressure [Pa]
dQ	differential change in heat present [J]
ds	differential change in entropy [J/kg]
dT	differential change in temperature [K]
d_w	distance to the nearest wall [m]
E	energy [J]
g	acceleration due to gravity [m/s^2]
h_{pr}	lower heating value of fuel [J/kg]
k	maximum dimple depth [mm]
$\dot{m}$	mass flow rate [kg/s]
P	pressure [Pa]
Q	heat transfer [J/s]
q	dynamic pressure [Pa]
R	gas constant [J/kg-K]
R	aircraft range [m]

s	entropy [J/kg]
T	temperature [K]
U	velocity [m/s]
W	work [J]
W	weight [N]

GREEK

Symbol	**Definition**
Δ	distance between cell center and nearest neighboring cell center [m]
γ	ratio of specific heats
η	efficiency
π	turbine stage total pressure ratio
τ	turbine stage total temperature ratio
ω	local total pressure loss coefficient

SUBSCRIPTS

Symbol	**Definition**
0-9	engine station numbering
0	stagnation or total
c	compressor
D	drag
L	lift
t	total
t	turbine

SUPERSCRIPTS

Symbol	Definition
^{o}	degree

ABBREVIATIONS

Symbol	Definition
ASC	Aeronautical Systems Center
BS	Bachelors of Science
CFD	computational fluid dynamics
DES	detached eddy simulation
LEBU	large eddy breakup
LES	large eddy simulation
LPT	low pressure turbine
MEMS	micro-electromechanical systems
MS	Masters of Science
MSRC	Mission Shared Resources Center
RANS	Reynolds-averaged Navier-Stokes
S-A	Spallart-Allmaras
T-S	Tollmien-Schlichting
TSFC	thrust specific fuel consumption
UAV	unmanned aerial vehicle
USNR	United States Naval Reserve
VBI	vane-blade interaction
VGJ	vortex generator jet

DETACHED EDDY SIMULATION ANALYSIS OF PAK-B LOW PRESSURE TURBINE BLADE

CHAPTER 1. INTRODUCTION

Currently, the Department of Defense uses Unmanned Aerial Vehicles (UAVs), like the Navy's X-47 Pegasus pictured in Fig. 1, for several missions such as high-altitude reconnaissance that have historically been performed by manned aircraft. As the technology advances, UAVs are likely to take on an ever-greater number of these missions. Unfortunately, the capability of UAVs to perform these missions, which often require flight at high altitudes and low velocities, is severely constrained by limitations inherent in low pressure turbines (LPTs), which provide power to the aircraft. Specifically, these flight conditions can result in an operating Reynolds number of less than 25,000. This operating condition causes the development of a laminar boundary layer over the turbine blades. The laminar nature of the boundary layer combined with the large turning angles generally associated with LPTs tends to cause flow separation over much of the turbine blade [Rouser,1]. This phenomenon limits the aircraft's range,

Figure 1: X-47 Pegasus UCAV [2]

altitude, and the amount of electrical power that can be extracted from the engine. Most current research emphasizes work on delaying or eliminating flow separation at low Reynolds numbers without adversely affecting blade performance at high Reynolds numbers.

Engineers at Pratt and Whitney® designed the Pak-B blade profile specifically to study and improve the performance of LPTs at low Reynolds numbers. The 2-D Pak-B shape comes from the 3-D Pak blade developed for commercial use at Pratt and Whitney. In order to analyze the Pak-B shape in 3-D space, the basic profile is extruded in the span-wise direction. However, though this blade design is useful for research purposes, it is not a commercially viable design since it neglects taper and twist [Rouser,1].

Lake [3] investigated passive flow separation control techniques on a Pak-B blade. He concluded that placing dimples on the blade just forward of the natural chord-wise separation location tends to prevent flow separation. Using this technique, he found that losses were reduced by 51.7% for a blade operating at a Reynolds number of 45,000

and freestream turbulence of 4%. Lake [3] hypothesized that the dimples acted as vortex generators. In effect, they energize the flow and force it to transition from laminar to turbulent before it reaches its natural separation point.

There are many advantages to passive control techniques such as the use of dimples. Unlike other methods, they have been shown to reduce operating inefficiencies at low Reynolds numbers and they do not adversely affect blade performance when operating at high Reynolds numbers [Rouser,1; Casey,4]. Also, they neither incur a weight penalty when compared to an unmodified blade nor do they require energy beyond the basic turbine requirement from the engine in order to operate. Furthermore, they can be retrofitted into existing designs without extensive redesign. Due to these advantages, the use of dimples for separation control produces favorable results. However, for future designs to effectively make use of this technique, a more complete understanding of the flow field and how it is affected by dimples is required.

The current research builds on previous studies into the effect of dimples on low pressure turbine blades. Two blade designs, an unmodified Pak-B blade and a Pak-B blade with a dimple positioned at 65% of axial chord, were computationally investigated using a recently developed turbulence model known as detached eddy simulation (DES).

1.1 Low Pressure Turbine Operation at Low Reynolds Numbers

Unlike other turbomachinery such as compressors or high pressure turbines, low pressure turbines are not generally subjected to extreme environmental conditions that require precautionary measures, such as active cooling, for safe operation. Therefore, research on low pressure turbines has tended to focus on optimizing their aerodynamic characteristics and maximizing their loading capabilities and efficiency. Research that

aims to improve the ability of low pressure turbines to operate at low Reynolds numbers falls into this category.

Low pressure turbines always operate in an unsteady environment. As they rotate, the turbine blades periodically shed wakes that generate high local freestream turbulence as they travel downstream. During these periods of high turbulence, the boundary layer generally does not separate from the blade. However, once a wake has passed and the turbulence decreases, the flow again becomes laminar and, as a result, more vulnerable to separation [Lake,2].

1.2 Previous Experiments in Flow Separation on LPT Blades

Numerous experiments dealing with low pressure turbines operating at Reynolds numbers below 200,000 have greatly enhanced our knowledge of the aerodynamics at these conditions. Sharma et al. [5] found that the loss coefficient increased dramatically when the operating Reynolds number dropped below 95,000. Murawski et al. [6] and Qiu and Simon [7] subsequently showed that operating at low Reynolds numbers significantly decreased the effectiveness of low pressure turbine blades. Specifically, Murawski et al. [6] noted separation from 75% to 90% of axial chord at Reynolds numbers as low as 53,000 and Qiu and Simon [7] verified that reattachment occurs downstream of 90% of axial chord. Simon and Volino [8] ran experiments on a Pak-B blade operating at flow conditions similar to those experienced by high-altitude reconnaissance aircraft and confirmed the decrease in effectiveness.

These research efforts created a foundation for Lake's [3] research with a Pak-B blade operating at low Reynolds numbers. Lake [3] showed that several indicators of effectiveness, including the total pressure loss coefficient and wake momentum deficits,

increased due to flow separation at these operating conditions. At a Reynolds number of 45,000, he discovered a natural separation location at 70% of axial chord [Lake,3]. Subsequently, he attempted to control separation with various devices, including trip wires, span-wise V-grooves, and recessed dimples. Though he noted a reduction in flow separation with each of these devices, he concluded that dimples most effectively reduced separation.

Rouser [1] further decreased the operating Reynolds number to 25,000 and experimentally investigated several other dimples patterns consisting of either full or stream-wise half-dimples located at 50%, 55%, or 65% of axial chord. Of these configurations, he found the most effective to be a row of full dimples located at 65% of axial chord. This design reduced the amount of separation by 28%. He also studied computational models of both an unmodified Pak-B blade and a Pak-B blade modified with both full and half-dimples located at 65% of axial chord in order to gain more knowledge of the flow structure. In his computational research, he utilized several viscous models, including a laminar solver and the Spallart-Allmaras, K-ω, and K-ε turbulence models. Rouser's [1] computational results described a highly transitional flow field. Unfortunately, the turbulence models amplified the instability inherent to the flow field so that they could not resolve a separation location. The laminar solver resolved the separation location at 66% of axial chord.

Casey [4] expanded the base of research by investigating several new dimple patterns. Experimentally, Casey [4] studied a row of dimples with a 2.22 cm center-to-center spacing located at 65% of axial chord, a row of dimples with a 4.44 cm center-to-center spacing located at 65% of axial chord, and a two-row staggered pattern with

dimples located at 65% and 76% of axial chord with a 4.44 cm center-to-center spacing. The results from each dimple pattern were compared to results from an unmodified blade at operating Reynolds numbers of 25,000, 45,000, and 100,000. He found that no dimple pattern performed significantly more effectively than any other dimple pattern and that each pattern reduced the average total pressure loss coefficient by 34% for an operating Reynolds number of 25,000 and a freestream turbulence of 1%. Casey [4] also created slightly modified computational models of these cases and solved each case using a laminar solver. These models allowed Casey [4] to create a visualization of the flow field. Comparisons to the experimental data verified the accuracy of the computational results.

1.3 Current Research Objectives

The objective of the current research is to investigate the ability of a numerical model called detached eddy simulation (DES) to resolve the flow field surrounding a low pressure turbine blade. In order to allow valid comparisons with Casey's [4] results, two blade geometries were analyzed: an unmodified Pak-B blade and a Pak-B blade with a spherical dimple located at 65% of axial chord. A unique grid was created for both of these blade geometries. Both grids employed periodic boundary conditions in both the span-wise and pitch-wise directions in order to simulate an infinitely long 2-D blade with a full span of dimples and an infinite linear cascade, respectively. Both grids were built in Gridgen® and solved in Fluent® on a time-accurate basis using the DES turbulence model. Post processing, including calculation of separation and reattachment locations, streamline visualization, velocity magnitude contour plots, and boundary layer profiles, was performed in Fieldview®.

1.4 Chapter Summary

Chapter 1 contains an introduction to the current research and some background regarding its origins. Chapter 2 discusses the theory behind the analysis of low pressure turbines, various methods used in attempts to suppress flow separation, and the theory and application of the DES turbulence model. Chapter 3 discusses the computational methodology and results. Chapter 4 sums up the conclusions of this thesis and provides recommendations for future work on this topic.

CHAPTER 2. BACKGROUND AND THEORY

The primary focus of this research is the advancement of the technology found in UAVs. Specifically, it is desired to enhance the operational capacities of these aircraft by optimizing parameters such as range, altitude, and endurance. In order to do so, methods by which turbine efficiencies can be increased were investigated. Pressure and velocity are the computational parameters most directly correlated with turbine efficiency. Therefore, pressure and velocity data were gathered from the simulations and used during data analysis.

The operational conditions experienced by the low pressure turbines used to operate UAVs often reach Reynolds numbers as low as 25,000. Previous research and experience has shown that the flow over the turbine blade separates under these conditions. Since it is believed that the efficiency of the turbine will increase if the amount of flow separation can be reduced or eliminated, this research investigates methods to minimize flow separation. These research goals require a detailed model of the behavior of the boundary layer. The computational investigation during the course of this research provides a model of the boundary layer as well as a picture of the rest of the flow field.

2.1 Low Pressure Turbine Performance Evaluation

The maximum range of an aircraft is often used as a measure of its engine performance. Breguet's range formula shows the inversely proportional relationship between aircraft range and the engine's thrust specific fuel consumption (TSFC):

$$R = -\frac{C_L}{C_D} \ln\left(\frac{W_{final}}{W_{initial}}\right) \frac{U}{TSFC} \frac{1}{g} \tag{1}$$

where U is the flight velocity, g is the acceleration due to gravity, C_D is the drag coefficient, C_L is the lift coefficient, R is the aircraft range, W_{final} is the aircraft's final weight, and $W_{initial}$ is the aircraft's initial weight [Mattingly,9:46]. The TSFC is given by:

$$TSFC = \frac{U}{\eta_o h_{pr}} \tag{2}$$

where η_o is the engine efficiency and h_{pr} is the lower heating value of the fuel used by the engine [Mattingly, 11:30]. Substituting this relationship into Breguet's range formula gives:

$$R = -\frac{C_L}{C_D} \ln\left(\frac{W_{final}}{W_{initial}}\right) \eta_0 h_{pr} \frac{1}{g} \tag{3}$$

These algebraic manipulations show that as the efficiency of the engine increases, the maximum range of the aircraft also increases. Since the increase in engine efficiency also reduces the amount of fuel required for any arbitrary range, improvements in engine efficiency can simultaneously increase aircraft mission effectiveness and reduce the amount of money that would otherwise need to be spent on fuel for the aircraft.

The Brayton cycle describes an ideal thermodynamic cycle for a gas turbine engine. See Fig. 2 for a graphical representation of the Brayton cycle and its associated T-S diagram, where T is the temperature and S is the entropy.

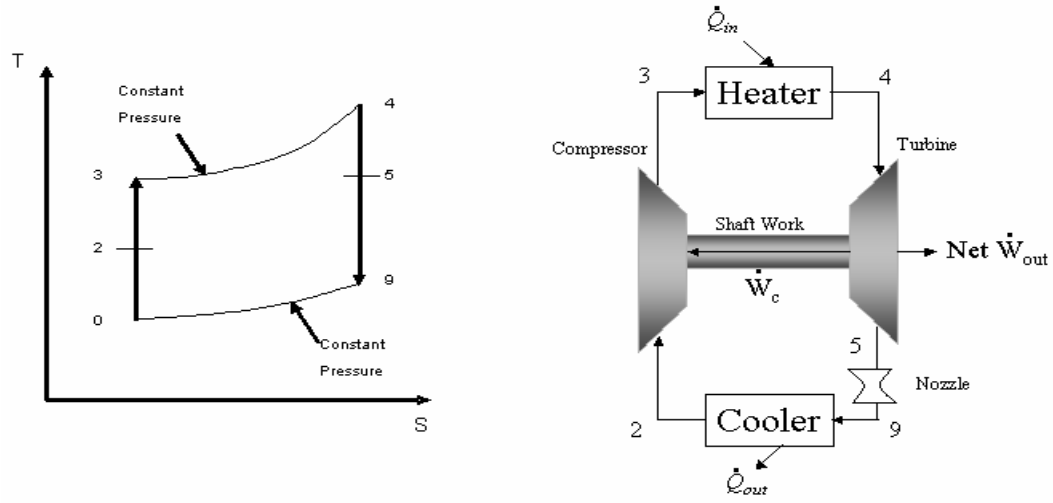

Figure 2: T-S Diagram and Illustration of Brayton Cycle [Mattingly, 9:233]

Between stations 0 and 3, the working fluid undergoes isentropic compression, resulting in an increase in both temperature and pressure, with the compressor mechanism located between stations 2 and 3. Between stations 3 and 4, it is then heated by the combustion of fuel injected into a combustor. This process takes place at a constant pressure and is often more simply modeled as a heat input as shown in Fig. 2. Then, between stations 4 and 9, the working fluid passes through a turbine and a nozzle, resulting in an isentropic decrease in both temperature and pressure. Then, between stations 9 and 0, the working fluid passes through another heat exchanger and rejects heat from the system. After passing through every station, the working fluid now has the same temperature, pressure, and entropy as it had before the cycle started [Oates, 10:136].

The first law of thermodynamics states that for a closed system:

$$\Delta E = Q - W \tag{4}$$

where ΔE is the net change in energy, Q is the heat added to or removed from the system, and W is the net work transferred into or out of the system [Moran and Shapiro, 11:58].

Assuming the working fluid is a calorically perfect gas, analysis of the Brayton cycle yields the following relationships:

$$\dot{W}_c = \dot{m}\ c_p\ (T_{t3} - T_{t2}) \tag{5}$$

$$\dot{W}_t = \dot{m}\ c_p\ (T_{t4} - T_{t5}) \tag{6}$$

where $\dot{W}$ is the rate that work passes through the system, $\dot{m}$ is the mass flow rate, c_p is the average specific heat at constant pressure, and T_t is the stagnation temperature [Mattingly, 11:234]. In the Brayton cycle, the work required by the compressor is supplied by the turbine so that $\dot{W}_c = \dot{W}_t$.

As stated previously, the Brayton cycle represents an ideal thermodynamic cycle. As such, it ignores the effects of entropy production. All real systems must also follow the second law of thermodynamics, which states that for a closed system:

$$ds \geq \frac{dQ}{T} \tag{7}$$

where ds is the net change in entropy and dQ is the net change in the amount of heat in the system [Anderson, 12:27]. Put simply, any real process will cause the entropy of the system and its surroundings to increase. Therefore, the Brayton cycle can only give an approximate representation of a gas turbine engine. A real turbine engine experiences losses due to many factors including flow separation, a potentially major factor in the overall engine efficiency.

A T-S diagram can illustrate a non-ideal system in the same manner that it described the Brayton cycle above. Fig. 3 shows a T-S diagram for a non-ideal turbine stage.

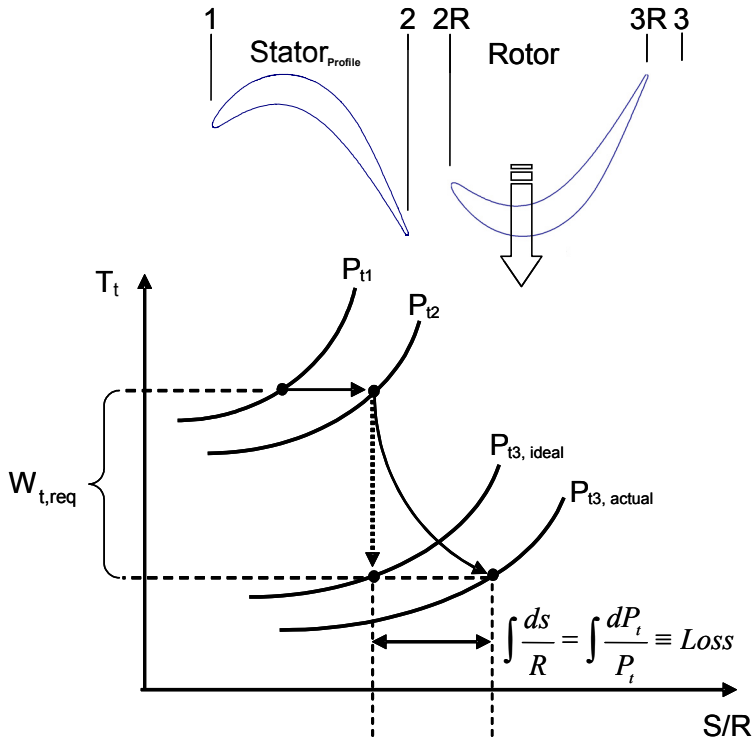

Figure 3: T-S Diagram for a Non-ideal Turbine Stage [Lake, 3]

As seen in Fig. 3, entropy increases over both the stator and the rotor. Furthermore, the pressure decreases over the stator and increases over the rotor. The Gibbs function relates the change in entropy to the changes in temperature and pressure:

$$ds = c_p \frac{dT_t}{T_t} - R \frac{dP_t}{P_t} \tag{8}$$

where ds is the change in entropy, R is the gas constant, c_p is the average specific heat at constant pressure, T_t is the stagnation temperature, dT_t is the change in stagnation temperature, P_t is the stagnation pressure, and dP_t is the change in stagnation pressure

[Oates, 10:38]. As seen in Fig. 3, the stagnation temperature is constant across the stator. Neglecting this term in Eq. 8 gives:

$$ds = -R\,\frac{dP_t}{P_t} \tag{9}$$

Eq. 9 describes the relationship between the pressure drop and the amount of entropy production across the stator. Logically, since there are relationships between pressure drop and entropy production and between entropy production and stage efficiency, it is also possible to directly relate pressure drop and stage efficiency:

$$\eta_t = \frac{1-\tau_t}{1-\pi_t^{\gamma_t - 1/\gamma_t}} \tag{10}$$

where η_t is the turbine efficiency, γ_t is the ratio of specific heats of the gases within the turbine, $\tau_t = \frac{T_{t3}}{T_{t1}}$, and $\pi_t = \frac{P_{t3}}{P_{t1}}$ [Oates, 221]. Assuming a fixed stagnation temperature ratio, decreasing the exit stagnation pressure, which can be measured within the linear cascade of a gas turbine engine, also decreases the turbine efficiency.

The total pressure loss coefficient, another measure of efficiency, is defined by the following equation:

$$\omega = \frac{P_{t,inlet} - P_{t,exit}}{q_{inlet}} \tag{11}$$

where ω is the total pressure loss coefficient, P_t is the stagnation pressure, and q_{inlet} is the dynamic pressure at the inlet [Casey,4]. As shown by Eq. 11, an increase in the exit stagnation pressure will decrease the total pressure loss coefficient. Since minimizing or eliminating the flow separation will increase the exit stagnation pressure, it will also decrease the total pressure loss coefficient. Lake [3] showed this effect in Fig. 4.

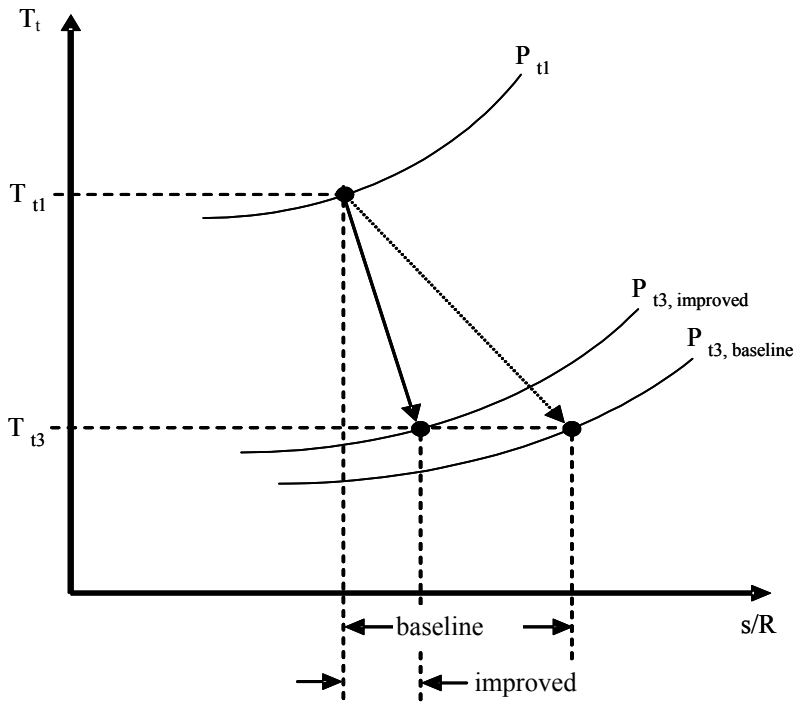

Figure 4: T-S Diagram Showing Improvements Due to Higher Exit Pressures [Lake,3]

The baseline plot represents a turbine with no surface modifications and the improved plot shows the significant improvement in efficiency that can result from only a small increase in the exit stagnation pressure.

In his research, Lake [3] found that dimples etched into the surface of a Pak-B blade reduced the total pressure loss coefficient. Later, Rouser [1] confirmed this result and showed that a dimple located at 65% of the axial chord had the greatest effect on increasing the engine efficiency. Casey [4] investigated several dimple patterns and found that each performed to a similar degree. Ultimately, he concluded that a single row of dimples at 65% of axial chord spaced 4.44 cm from each other produced the best results at the lowest cost [Casey,4].

2.2 Low Pressure Turbine Boundary Layer Aerodynamics

The flow fields about low pressure turbine blades are inherently unsteady and transitional. Halstead et al. [13;14] showed that turbulence levels between 1% and 20% exist in the freestream. They also detailed other structures within the flow field such as passing wakes, centrifugal effects, and vortices. Various researchers have shown that the boundary layers on low pressure turbine blades operating at low Reynolds numbers generally transition from laminar to turbulent over the suction surface of the blade [Mayle,15; Addison and Hodson, 16]. This transition is almost steady but is affected by time-dependent wakes caused by the relative motion of the rotor and the stator. As these wakes move downstream, the regions through which they pass quickly switch from transitional to turbulent and back to transitional once the wakes have moved on.

2.2.1 Experimental Laminar-to-Turbulent Boundary Layer Transition

Many researchers have focused their work on efforts to determine the exact location of transition and the length of the blade surface under the transitional region in order to determine a relationship between the duration of transition and performance losses. These variables are determined primarily by the transitional modes of the flow field. Walker [17] identified these modes as natural transition, bypass transition, and separation bubble transition. Unfortunately, since many factors can affect these transitional modes, including Reynolds number, freestream turbulence, and pressure gradients, research on this topic has been slow and difficult.

Each of these modes exists under very different conditions. Natural transition only occurs in flow fields characterized by low freestream turbulence and the absence of adverse pressure gradients. This process is initialized by the formation of two-

dimensional Tollmien-Schlichting (T-S) waves. As the flow progresses and the T-S waves become unstable, they create three-dimensional loop vortices and large fluctuations [Mayle, 15]. These structures merge and become turbulent spots that increase in size as they move downstream until they fill the entire boundary layer. At that point, the flow is considered fully turbulent.

Flow fields with freestream turbulence levels of approximately 20% or higher tend to experience bypass transition. T-S waves do not form in these flow fields but the higher level of turbulence still allows the formation of turbulent spots similar to those formed by natural transition. Walker [17] showed that linear stability theory could still be used to model these flow fields and the disturbances within them so that the length of the transitional region can be determined.

A laminar flow field characterized by adverse pressure gradients often sees the development of separation bubbles in which transition occurs in the shear layer between the freestream and the separation bubble. Separate investigations by Mayle [14] and by Qiu and Simon [8] confirmed that reattachment of the boundary layer to the blade surface is caused by the transition of the flow field from laminar to fully turbulent. This transition mode characterizes the flow field of a Pak-B blade operating at low Reynolds numbers.

2.2.2 Numerical Models for Low Pressure Turbine Performance

Previous numerical studies of low pressure turbines have been hindered by the inability of the models used to resolve the flow field. This difficulty has been attributed to the absence of experimental research to compare with those numerical models [Werle, 18]. Halstead et al. [19] attempted to use many different models, including STANX,

KEP, Navier-Stokes, and Fan-Lakshminarayana, that ultimately failed to produce realistic results. Lake [3] used the two-dimensional Allison Vane-Blade Interaction (VBI) code. He found that though this code generally worked well, it still had difficulties resolving the separated region at low Reynolds numbers and was unable to deal with three-dimensional flow structures characteristic of the flow fields surrounding dimples. As such, he used this code for an unmodified Pak-B blade only.

For his research, Lake's [3] computational model included an O-grid around the blade and an H-grid in the blade's passage. Rouser [1] built on Lake's [3] model in order to create a three-dimensional grid. He extruded a structured O-grid from the surface of the blade to produce hexahedral cells in the near-wall region. He then modeled the blade passage using an unstructured grid characterized by tetrahedral cells. The flow region directly above the dimples was also modeled using an unstructured grid style. However, this region used prism cells instead of hexahedral cells and extended all the way to the wall. See Fig. 7 for an illustration of these cell types.

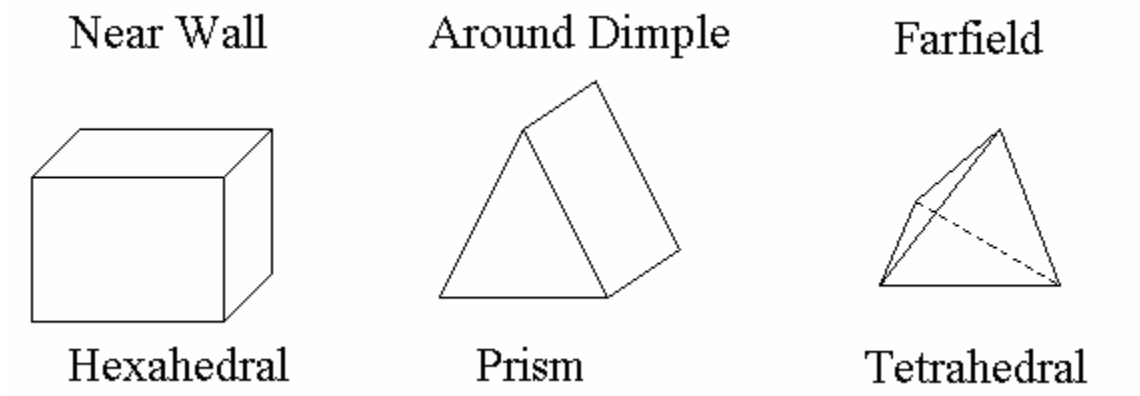

Figure 5: Illustration of Cell Types [Casey,4]

After building the grid, Rouser [1] computed the flow field in Fluent®. Initially, he assumed a turbulent flow and employed a Reynolds Averaged Navier-Stokes (RANS) turbulence model throughout the domain. He found that the RANS model predicted that no separation would occur in a flow field with an inlet turbulence level of 1%. After developing this solution, Rouser [1] switched to a laminar solver and discovered that it could properly resolve the flow field at the separation and reattachment locations but was unable to do so in the turbulent region aft of the reattachment point. He surmised that a new turbulence model able to resolve this region properly was necessary.

Casey [4] used the same overall grid style as Rouser [1]. However, rather than attempt to use a turbulence model, he computed the flow field using a time-accurate laminar solver since he believed this to be more physically accurate than running the laminar solver from a steady turbulent solution as Rouser [1] had done. This approach was more successful than previous attempts to describe the flow field. Unlike Rouser [1], Casey [4] resolved large vortical structures in the flow field with a dimpled blade.

Rizzeta and Visbal [20] performed a computational investigation using the large-eddy simulation (LES) turbulence model on an unmodified Pak-B blade with operating Reynolds numbers as low as 25,000. They found that the LES turbulence model was able to capture the features of the transitional flow field. Also, their results, which included variables such as coefficient of pressure, mean velocity, and fluctuating velocity, compared fairly well with a two-dimensional model of the blade. However, the LES model did not provide perfect results. The coefficient of pressure data differed from experimental data although they attributed this error to the non-periodic nature of the experimental data. Prasad et al. [21] used the LES model to resolve the flow field for an

HEV static mixer and discovered that, whereas previous turbulence models could not resolve experimentally observed vortices, the LES model predicted their existence.

The current research employed a turbulence model called detached eddy simulation (DES) throughout the flow field. DES is a hybrid model that applies different numerical turbulence models to different regions of the grid. Specifically, it uses a RANS turbulence model in the boundary layer and a large-eddy simulation approach outside of the boundary layer. The DES model used in this research is based on the Spallart-Allmaras (S-A) turbulence model. In order to modify the S-A model, the DES model replaces the S-A variable d_w, the distance to the nearest wall, with:

$$\tilde{d} = \min(d_w, C_{DES}\Delta) \tag{12}$$

where C_{DES} is the DES model constant and Δ is the largest distance between the cell center being considered and the cell center of its neighbors [Kapadia et al., 22]. Inside the boundary layer, $\tilde{d} = d_w$ and the normal S-A model operates so that RANS calculations are made. Otherwise, outside the boundary layer, the model becomes grid-scale dependent and switches to the LES turbulence model [Kapadia et al., 22].

Due to the relative newness of the DES model, gridding practices are still somewhat underdeveloped. Spalart [23] provides fairly complete instructions and defines three specific flow regions within any grid that need to be gridded appropriately in order to obtain the most physically accurate results in the most cost-effective manner: the Euler region, the RANS region, and the LES region. The Euler region is located upstream and to the sides of the object being modeled and contains no turbulent flow. This region should generally have the greatest volume but the least number of grid points and is marked by even, isotropic grid spacing. The RANS region contains the boundary layer

including the initial location of separation and consists of inner viscous sub-region and an outer sub-region. The inner sub-region should be modeled in the same manner as a full-domain RANS. In the outer sub-region, the grid spacing is allowed to expand such that the spacing ultimately equals that of the adjoining Euler region. As such, this region fulfills the needs of numerical robustness rather than any physical requirement. The LES region is the primary region containing turbulence and consists of three sub-regions: the viscous sub-region, the focus sub-region, and the departure sub-region. The viscous sub-region is modeled in the same manner as the viscous sub-region of the RANS region. The focus region sits close to the object being modeled and it is important that the turbulence be accurately resolved here so fairly tight grid spacing is required. In the departure region, the spacing expands significantly since the structure of the turbulence is no longer as important.

2.3 Separation Control on Low Pressure Turbines

Research by Murawski et al. [6] and Qiu and Simon [7] has demonstrated that Reynolds numbers below 300,000 or freestream turbulence below 10% more easily allows separation than operating conditions above these values. Generally, both conditions are met by the mission profile of a high-altitude reconnaissance aircraft. As the Reynolds number decreases, the transition location on the blade moves downstream until it is far enough that the flow field cannot follow the curvature of the blade and separation occurs. Many researchers have investigated methods by which low pressure turbine blades can be modified to minimize the amount of separation.

2.3.1 Active and Passive Flow Separation Control Methods

Separation control methods can be classified as either active or passive. The operation of active controls requires an input of energy whereas passive controls do not. Rather, passive control methods generally involve modifications to the surface of the turbine blade. On the other hand, active controls can be switched on or off or adjusted for intensity as conditions require whereas, once instituted, passive controls cannot be adjusted. Ultimately, the advantages of active controls make them better suited to flow fields with varying conditions while passive controls are better suited to flow fields with fairly steady operating conditions.

Johnston and Nishi [24] and Compton and Johnston [25] showed that vortex generator jets (VGJs) control separation on flat plates subjected to adverse pressure gradients. Bons at al. [26] investigated the interactions between VGJs and a Pak-B blade and found that pulsating VGJs operate as effectively as steady VGJs with less mass flow. Unfortunately, this type of active control requires the costly input of high pressure air between the turbine and the compressor. Furthermore, they add weight to the engine and can easily become clogged by combustor exhaust particles. As such, they require more maintenance to remain effective. Borgeson [27] attempted to use micro-electromechanical systems (MEMS) to delay separation over a cylinder. Though he met with some success, this method cannot currently be effectively used with a low pressure turbine due to the inability of MEMS to withstand extreme operating conditions and the difficulty associated with installing these devices in a low pressure turbine blade.

Passive controls tend to be cheaper, easier to use, and better able to withstand harsh operating conditions. Furthermore, by improving the ability of current blade

designs to avoid separation, they prevent costly redesigns that can adversely affect the efficiency of low pressure turbine blades in other ways.

The most common passive control techniques are modifications to the surface of the low pressure turbine blade. Lin et al. [28] found that large-eddy breakup (LEBU) devices reduced separation at small positive angles of attack. They also showed that vortex generators submerged within the blade effectively suppressed separation so long as the device had the correct height and was properly positioned relative to the natural separation location of the blade surface. Austin [29] and Gamerdinger and Shreeve [30] researched triangular plow vortex generators and found that they reduced shock-induced separation. Unfortunately, these devices also reduced downstream stagnation pressures. Rao and Kariya [31] looked at submerged semi-circular and simple vane vortex generators. They found that the submerged devices performed better than the vane devices as long as their design included the correct height, sweep angle, spacing, and length. See Fig. 6 for illustrations of these passive control devices.

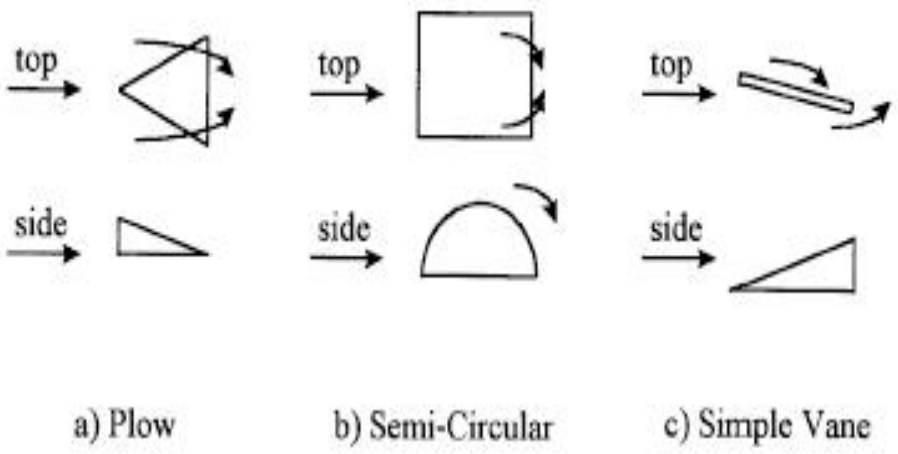

Figure 6: Surface Vortex Generator Devices [Lake,3]

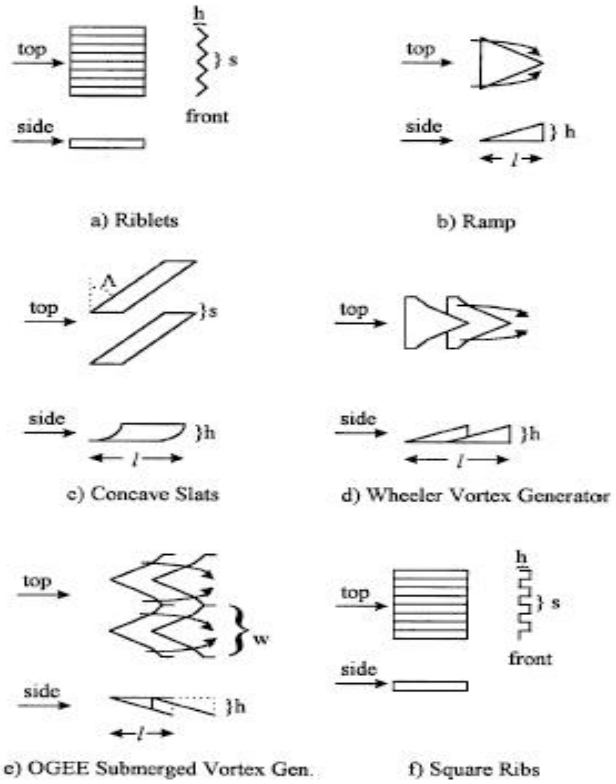

Figure 7: More Vortex Generator Devices [Lake,3]

Due to the interactions between the flow field and the protruding structures discussed, these devices incur a drag penalty that offsets many of the performance enhancements gained by the reduced separation. Lin et al. [32] proposed several alternatives to these protruding structures designed to reduce the drag penalty including a $\pm 45^{o}$ small-scale riblet pattern and transverse grooves. The transverse grooves successfully reduced separation while the riblet pattern actually increased the amount of separation. McCormick [33] proposed a passive cavity method that uses the adverse pressure gradient behind the separation location to assist in reducing separation. He found that this idea reduced the stagnation pressure loss but contributed to the deterioration of the boundary layer.

Other separation control ideas include leading edge vane vortex generators, small-scale V-groove riblets, small-scale square ribs, and a vortex generator shaped like a NACA 64-812 airfoil [Casey,4]. Unfortunately, all of these techniques are very difficult to use. Bloch and Mueller [34] investigated roughness strips placed near the leading edge of an airfoil that are much easier to install. Lake [3] examined three passive control techniques: a V-groove channel, a boundary layer trip wire, and dimples. He found dimples to be the most effective separation suppression technique but also found that their effectiveness was highly dependent on several factors including the position of the dimple relative to the separation location. Rouser [1] and Casey [4] both confirmed this conclusion and concluded that the best location for the dimple was at 65% of the axial chord.

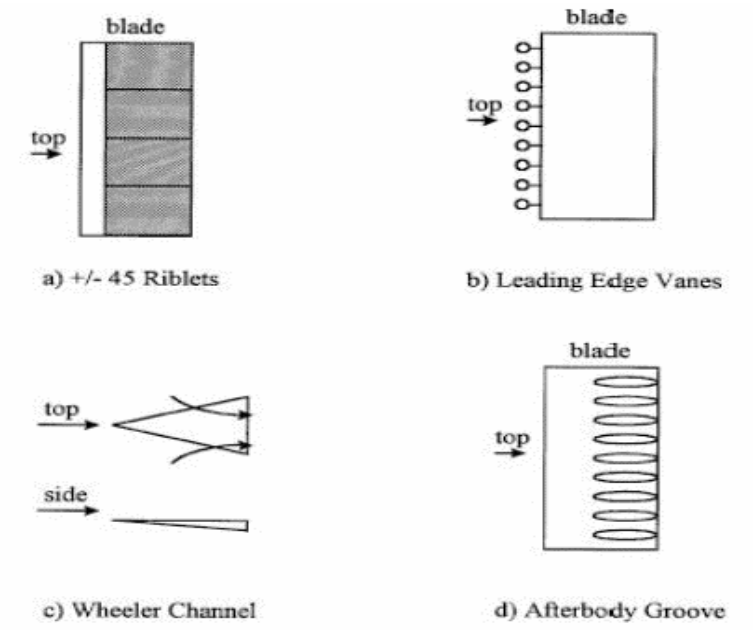

Figure 8: More Vortex Generator Devices [Lake,3]

2.3.2 Previous Research in Dimples for Boundary Layer Control

Both submerged and protruding vortex generators have been shown to suppress boundary layer separation. Protruding surface modifications entrain air from the freestream into the boundary layer, thereby energizing it and reducing the amount of separation [Taylor, 35]. Also, vortices shed off the leading edge which mixes the freestream and the boundary layer downstream. On the other hand, submerged vortex generators do not incur as severe a drag penalty as the protruding modifications. Advantageously, they are easier to install on low pressure turbine blades and can handle harsher environmental conditions. But, they are less effective unless placed very near the separation location. Lake [3], Rouser [1], and Casey [4] have all shown the strong potential that dimples have in boundary layer control applications.

Research has generally confirmed that recessed dimples reduce the amount of separation in the boundary layer. Therefore, more recent research has focused more on the factors that can affect the effectiveness of dimples more than the viability of dimples themselves. Bearman and Harvey [38] investigated spherical and hexagonal dimples on a sphere and demonstrated that both shapes generated downstream vortices. Of the two, they found that the hexagonal dimple shape operated more efficiently.

In his research, Lake [3] built on the procedures and results of Bearman and Harvey [38]. He milled dimples into a Pak-B blade with the same roughness characteristics as Bearman and Harvey [38]had previously used ($k/D = 9 \times 10^{-3}$ where k is the maximum dimple depth and D is the spherical diameter). Lake's [3] dimples were drilled with a 5.08 cm ball end mill to a depth of 1.588 mm. Ultimately, they took elliptical shape due to the curvature of the blade with a chord-wise length of 15.13 mm

and a span-wise length of 17.53 mm with a center-to-center spacing of 2.22 cm. Lake [3] installed dimples at three axial chord locations (50%, 55%, and 65%) and researched them using a linear cascade of eight blades with the dimpled blade in the fifth position. He tested operating conditions with Reynolds numbers of 50,000, 100,000, and 200,000. Each case led to a loss reduction for the blade.

For his research, Rouser [1] used the same blade as Lake [3]. He repeated each of Lake's [3] cases down to Reynolds numbers of 25,000. He also experimented with asymmetric dimples by filling half of each dimple with Playdoh® in the span-wise direction. Ultimately, he concluded that the full dimples at 65% of axial chord performed most efficiently.

Casey [4] also used the same blade as Lake [3] and Rouser [1]. In order to test the effectiveness of multiple rows of dimples, he drilled another row of dimples identical to the row at 65% of axial chord at 76% of axial chord. He also looked at a single row of dimples at 65% of axial chord with 4.44 cm spacing rather than the 2.22 cm spacing previously used by Lake [3] and Rouser [1]. He found no appreciable differences between the different dimple patterns and concluded that, for ease of manufacturing, the single row at 65% of axial chord with a 4.44 cm dimple spacing was the best choice for boundary layer control.

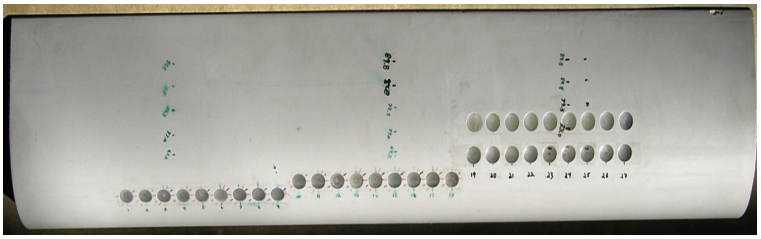

Figure 9: Experimental blade after modification by Casey with dimples at 50%, 55%, 65%, and 76% of axial chord

CHAPTER 3: COMPUTATIONAL STUDY

Originally, Rouser [1] created a computational model for an unmodified Pak-B blade. To do so, he constructed a two-dimensional grid from a set of coordinates known to define the Pak-B profile. Then, the two-dimensional grid was extruded span-wise to create a three-dimensional grid model of the basic Pak-B shape. His grid included structured grids on the blade surface and within the boundary layer and unstructured grids in the rest of the blade passage. The baseline grid developed by Rouser [1] was modified to create the grid used in this research. The grid topology is discussed in greater detail in section 3.2.

The grid model was simulated with an axial inlet Reynolds number of 25,000. A time-accurate solution was developed using the detached eddy simulation turbulence model.

The purpose of this research is to run several cases using the detached eddy simulation turbulence model and determine the ability of the model to make computations for use in predicting future results from experiments for this application. Also, the results may enhance knowledge of the physics surrounding flows around low pressure turbine blades and within dimples on these blades. Unfortunately, the three-dimensional grids used for this research do not represent actual physical structures. They neglect the effects of blade characteristics such as taper, twist, and the blade's rotating motion. Therefore, the CFD analysis will accurately model the flow field only on the mid-span of the blade. Furthermore, to enhance the two-dimensional effects, the blade is modeled with an infinite span and the cascade is modeled with an infinite number of

blades. Ultimately, the primary reason for this research is to better visualize the flow field and flow structures within the field.

3.1 Computational Software

Three commercial software packages were used during the course of this research: Gridgen® v15, Fluent® v6.1.22, and Fieldview® v9. Gridgen® is a grid generation software package designed to interface with various CFD packages. The research grids were created and modified in Gridgen®. This can be a delicate process since the software packages will not accurately model the flow field without a proper grid. Each node within the grid represents a point in space at which the governing equations are solved. Grids are created by properly placing these nodes within the various regions that make up the grid. If the grid points are placed too far apart, the solver cannot accurately resolve the flow field. On the other hand, if the grid points are too near each other, the number of cells increases dramatically and a prohibitive amount of memory and computing time is necessary. There are two types of grids: structured and unstructured. On structured grids, the number of grid points on opposing boundaries must be the same and a grid point on one boundary corresponds to a grid point on another boundary. Neither of these requirements must be met for unstructured grids.

Gridgen® was also used to set boundary conditions for the grid models. Each case used a velocity inlet boundary condition where the flow enters the blade passage and a pressure outlet condition where the flow exits. Also, both the pitch-wise and span-wise faces of the grid were set with periodic boundary conditions in order to simulate the infinite linear cascade and the infinite length of the blade, respectively. The span-wise periodic boundary condition simulates an infinite row of dimples on the blade.

After the grid was created, it was saved as a Fluent® case file from which the flow field can be resolves. Fluent® uses a finite volume method to discretize and solve the Navier-Stokes equations for the flow field. Finite volume methods are derived from the integral form of the equations of motion and then solved by the application of the conservations laws. Each cell within the grid makes up a finite volume in which all flow properties are assumed to be constant. In each finite volume, physical quantities such as mass must be conserved. Fluent® makes these calculations by integrating density in each cell to determine its instantaneous mass. The time rate of change of this calculated mass equals the mass flux through the cell. These rates are then mathematically analyzed based on the properties in adjacent cells to determine flow properties of each of the cells in the domain.

Solutions were computed with the following boundary conditions. The inlet velocity components were 1.77804 m/s in the x-direction and 1.221704 m/s in the y-direction. This corresponds to an inlet angle of 34.5^{o}. The inlet pressure was set to 101,325 Pa and the outlet pressure to -4.4 Pa. The no-slip condition was set at the blade surface. The DES model constant was set at the default value, 0.65.

Each grid utilized Fluent's® unsteady solvers to create a time-accurate solution. For the unsteady solver, the time step is set to a constant value for every cell within the grid. Though this leads to a more accurate transient solution than the steady solvers can provide, it also requires that the time step be set to a level low enough to resolve the most time-sensitive region of the flow field. The unsteady solver computes as many time steps as the user requires with a set maximum number of iterations per time step. If the convergence criteria set by the user are met during the computations for any particular

time step, the particular time step cuts short and the solver proceeds to the next time step. For this research, the time step was set to .00005 s and the convergence criteria was 10^{-6}. The cases were run on the Compaq® CS40/45 at the Mission Shared Resources Center on between 24-32 processors per case.

Post processing operations were performed in Fieldview®, which is more functional than Fluent® in that regard. While running the solutions in Fluent®, the files were set up to write out Fieldview® case and data files every .00075 s of flow time, which corresponds to 15 time steps. This allows the user to analyze the flow field at a particular instant in time or over many time steps during the run. Fieldview's® capabilities include calculations of the separation and reattachment locations, velocity contours, and visualization of the flow field using streamlines.

Fieldview® was also used to make calculations and show diagrams of the boundary layer. To do so, the velocity magnitude was plotted along a 2-cm vector normal to the surface of the blade at its mid-span. The boundary layer measurements were taken at 67.2%, 73.0%, 79.3%, 84.8%, and 89.8% of the axial chord.

3.2 Grid Characteristics

Initially, a file containing the coordinates that describe a Pak-B profile was imported into Gridgen®. This profile was extruded in a span-wise direction to create a three-dimensional blade with the Pak-B shape and a span of 11.28% of axial chord. Both grids were composed of both structured and unstructured regions. In both cases, the surfaces of the blade and the boundary layer around the blade were constructed using a structured grid. These models included quadrilateral cells on the surface transitioning into hexahedral cells within the boundary layer region. As the distance from the blade

surface increased, the grid model transitioned to an unstructured format filled with tetrahedral cells. For the dimpled grid model, the dimple surface was modeled by triangular cells. When these were extruded into the unstructured region above the dimple, the cells became prisms.

3.2.1 Grid Topology for Unmodified Pak-B Blade

For the unmodified blade, the grid that Rouser [1] created in his research was modified for the DES turbulence model. The solution was resolved on the Compaq® CS40/45 at the MSRC on 24-32 processors to a flow time of .35 s. On this grid, 51 nodes were placed across the span. To better resolve flow structures, a higher cell density was desired in regions where high flow gradients were expected. Therefore, more cells were located near the leading edge and the trailing edge and near the separation location and over the suction surface of the blade. The Pak-B shape is defined by 517 nodes. The grids on the blade surface were then extruded normal to the blade to create the boundary layer region. This region includes 51 nodes on the normal vector starting with a spacing of .000080356 m. The spacing grows as the distance from the blade increases with a growth rate of 1.1. The surface of this domain is then extruded again to enclose the remainder of the expected turbulent region as required by the DES model. This region includes 16 nodes along the vector normal to the blade and has an initial spacing of .010178 m. The spacing increases with a growth rate of 1.25. The outer boundary of the outlying unstructured region includes 15 nodes pitch-wise, 5 nodes span-wise, and 231 nodes stream-wise. Ultimately, the grid for the unmodified blade includes 1,801,522 nodes and 3,897,601 cells. These values represent an increase of about 1 million nodes and 2.5 million cells over the grid originally created by Rouser [1]. The primary

modifications include doubling the thickness of the structured region near the wall to ensure that it captured the turbulent structures in the flow field and increasing the number of grid points in the boundary layer region near the wall to more accurately resolve flow field characteristics in this region.

3.2.2 Grid Topology for Pak-B Blade with Dimple at 65% of Axial Chord

For the dimpled blade, the grid that Casey [4] created in his research was modified for the DES turbulence model. The solution was resolved on the Compaq® CS40/45 at the MSRC on 24-32 processors. Casey [4] created a spherical database structure with a diameter of 5.08 cm and merged it with the database for the unmodified blade. By cutting the sphere at the intersection between its surface and the blade surface and creating a domain on the surface of the spherical database structure, Casey [4] created a domain on the dimple centered at 65% of axial chord and with a depth of 1.588 mm. The line of intersection between the blade surface and the sphere contained 360 equally spaced nodes. Above the dimple, an unstructured region was included to the same height as the boundary layer region around the rest of the blade. The dimple shape was extruded through this region so that the top face included it. Above this region, another unstructured block was created to the same height that the turbulent region was modeled above the rest of the block. This region did not include the dimpled shape. Ultimately, the grid for the dimpled blade included 2,899,416 nodes and 5,020,832 cells. These values represent an increase of about 1 million nodes and 2 million cells over Casey's [4] grid. The primary modifications include doubling the thickness of both the structured region near the wall and the unstructured region above the dimple in order to ensure that it captured the turbulent structures of the flow field.

Fig. 10 illustrates the basic grid for the mid-span of the blade passage for each case.

Fig. 11 illustrates the basic grid in the boundary layer for each case.

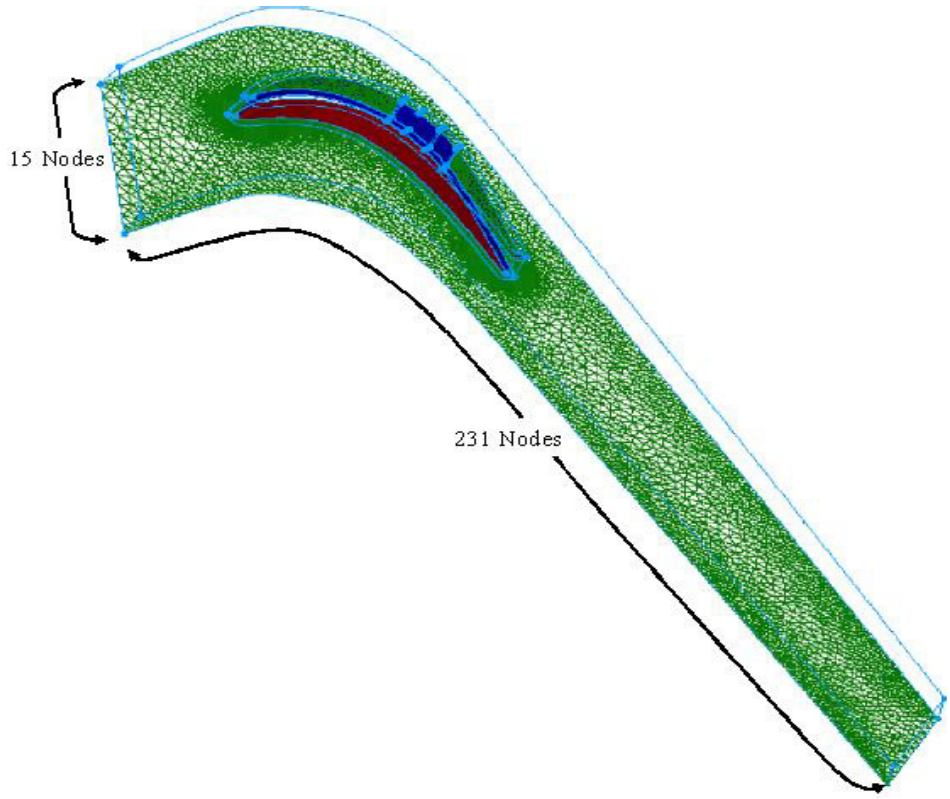

Figure 10: Grid topology of Pak-B mid-span passage [Rouser,1]

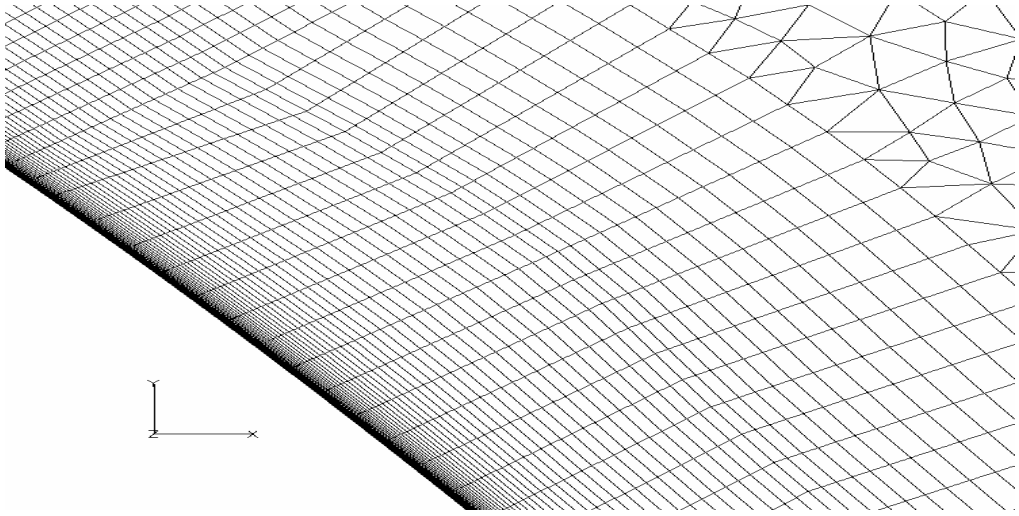

Figure 11: Grid topology of boundary layer

3.3 Computational Results for Pak-B Unmodified Blade

3.3.1 Separation Location

Fig. 12 shows a diagram of the locations of separation and reattachment as calculated by Fieldview®. To provide a sense of perspective, the green dots are located at 67.2%, 73.0%, 79.3%, 84.8%, and 89.8% of axial chord. The diagram indicates that no separation occurs until the flow field has passed 89.8% of axial chord. It also indicates that the flow attempts to reattach to the blade surface at many positions although there are no reattachment locations that totally the blade surface. Rather, the reattachment lines follow the direction of the flow. For comparison, Casey [4] found that Fieldview® calculated the location of separation for an unmodified blade at between 64.5% and 68.5%.

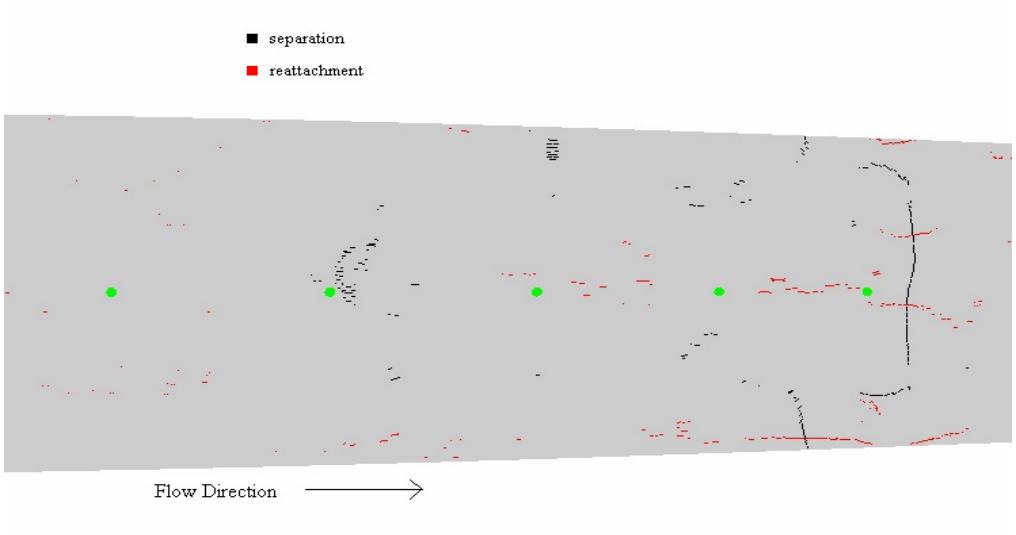

Figure 12: Separation and reattachment locations for unmodified Pak-B blade run at Re 25k using DES turbulence model at 0.3495 s

3.3.2 Velocity Profile

Fig. 13 shows the velocity magnitude contours of the computational flow field for an unmodified Pak-B blade on a plane located at the mid-span of the blade. It illustrates the presence of vortical structures within the turbulent region of the flow field as indicated by the increase in velocity contained within the separated region. Also, Fig. 11 shows that the flow separates from the blade surface at the position where the boundary layer begins to move away from the blade. Note that this position is much farther upstream than the position that Fieldview® calculated for separation. The separated region of the flow field steadily increases in size beginning at the location of primary separation. Though the rate of growth slows as the flow moves downstream, the separated region appears to grow in size until the flow reaches the trailing edge of the blade. Span-wise uniformity of the contour plots were checked and no significant differences were discovered.

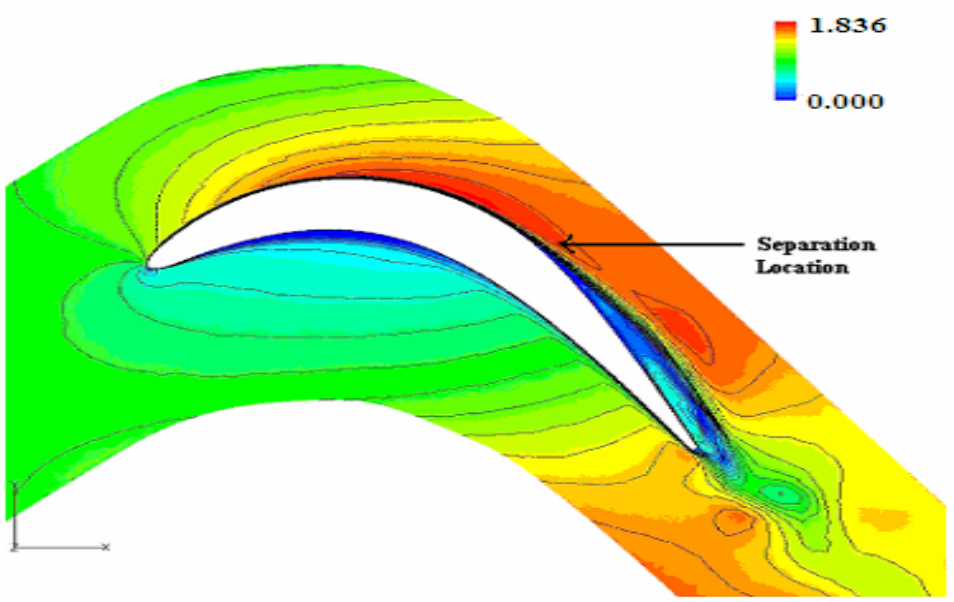

Figure 13: Contour plot of normalized velocity magnitude for unmodified Pak-B blade at Re 25k using DES turbulence model at 0.3495 s

Fig. 14 shows a close-up of the vector field that defines the turbulent region of the flow on a plane located at the mid-span of the blade. A large vortical structure shedding from the blade dominates this region of the flow field. Fig. 15 depicts another close-up of the vector field nearer the blade surface. The red lines located beneath the vector field illustrate that the flow attempts to reattach to the blade surface within the turbulent region. The large backflow present within the turbulent region of the flow field rejects the attempts of the boundary layer to reattach. It is likely that the previously noted vortical structure has a large effect on these reattachment attempts since, as evidenced by the greater density of reattachment lines, the reattachment occurs more strongly immediately after the vortical structure passes downstream. These results match previous research performed by Halstead et al. [3] and Casey [4].

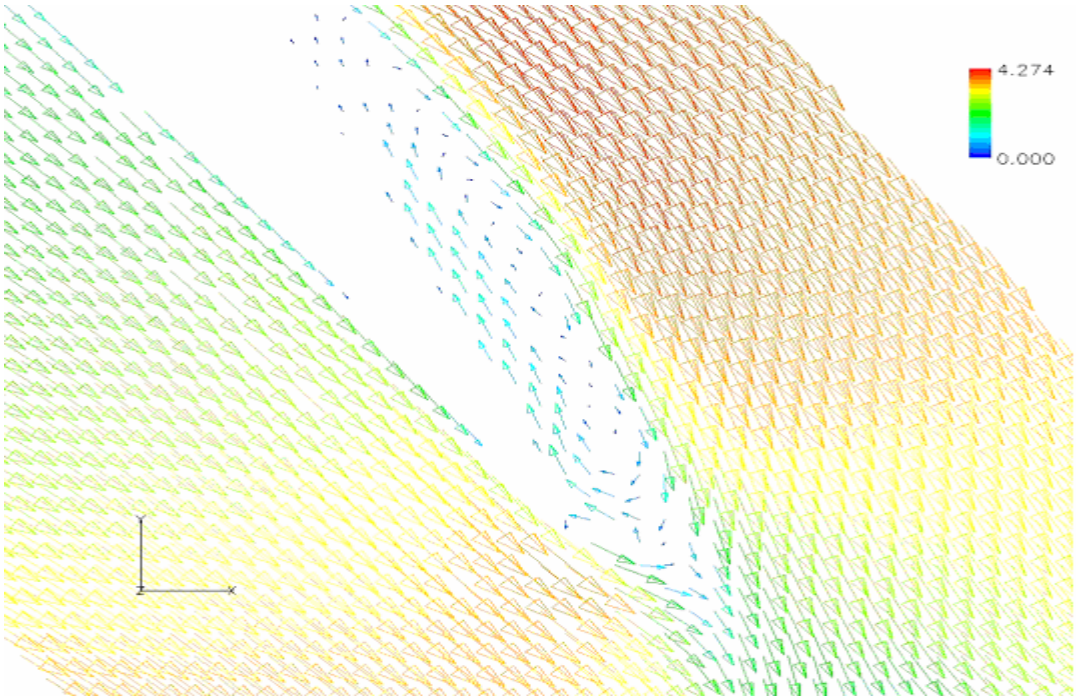

Figure 14: Vector plot of velocity magnitude in turbulent region for unmodified Pak-B blade at Re 25k using DES turbulence model at 0.3495 s

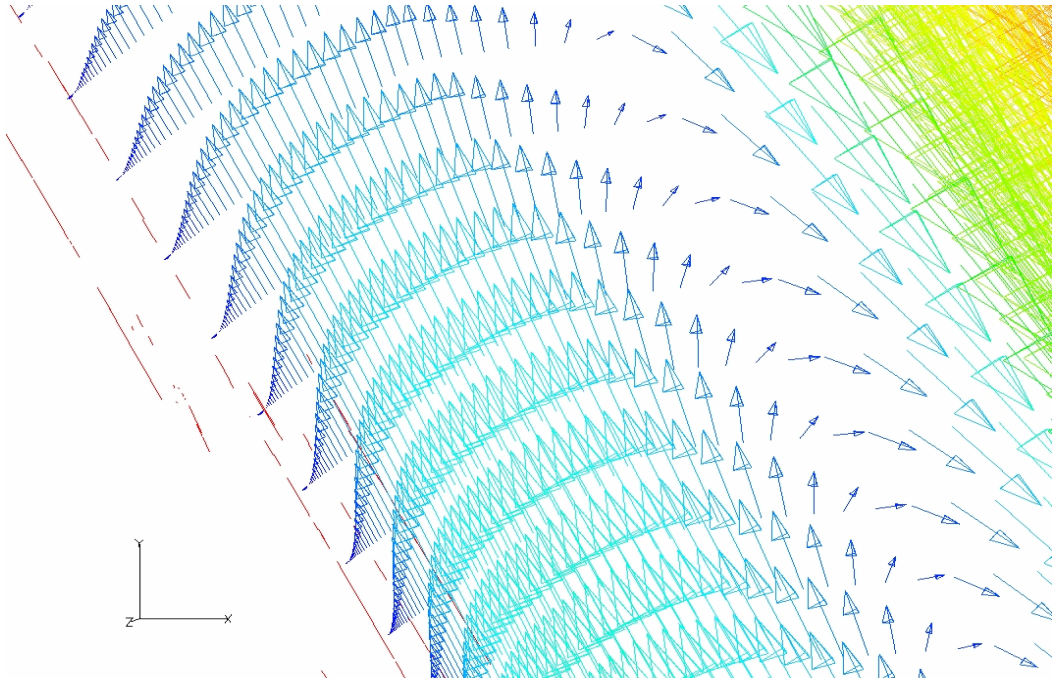

Figure 15: Vector plot of velocity magnitude in turbulent region for unmodified Pak-B blade at 25k using DES turbulence model at 0.3495 s

3.3.3 Streamline Visualizations

Fig. 16 shows a side view of a set of surface streamlines along the entire span of the blade. The streamlines show definite separation from the blade surface between 65% and 70% of axial chord.

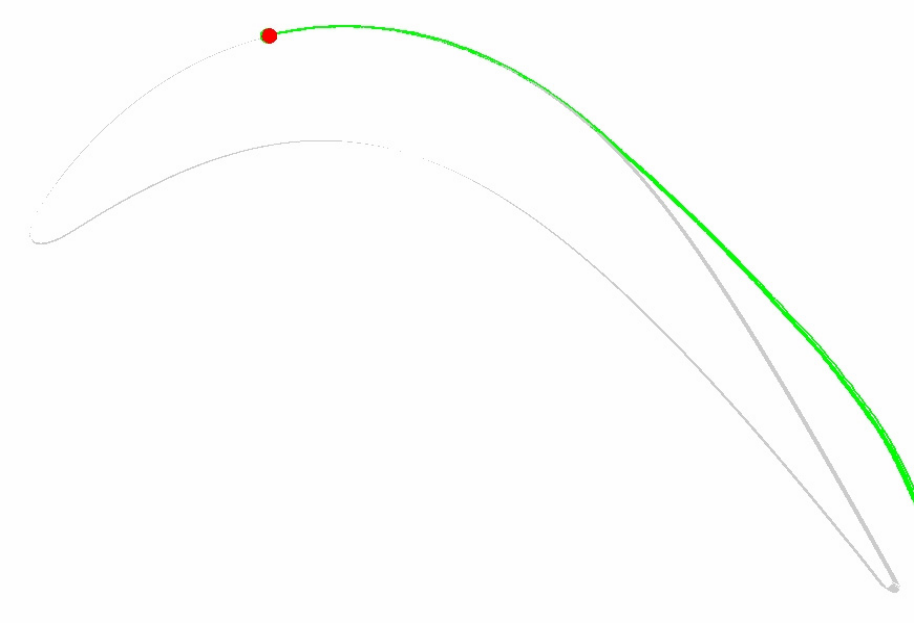

Figure 16: Streamline visualization of flow field for unmodified Pak-B blade at Re 25k using DES turbulence model at 0.3495 s of flow time

3.3.4 Computational Boundary Layer Measurements

Fig. 17 shows profiles of the boundary layer constructed for the unmodified Pak-B computational model along the mid-span of the blade. At 67.2% of axial chord, there is a very slight inflection point located near the blade surface. That inflection point indicates that the flow has already begun to separate from the blade surface at this location. At 73.0 % of axial chord, there is a small separation bubble forming in the flow field. As the flow moves downstream, the separation bubble steadily grows in size.

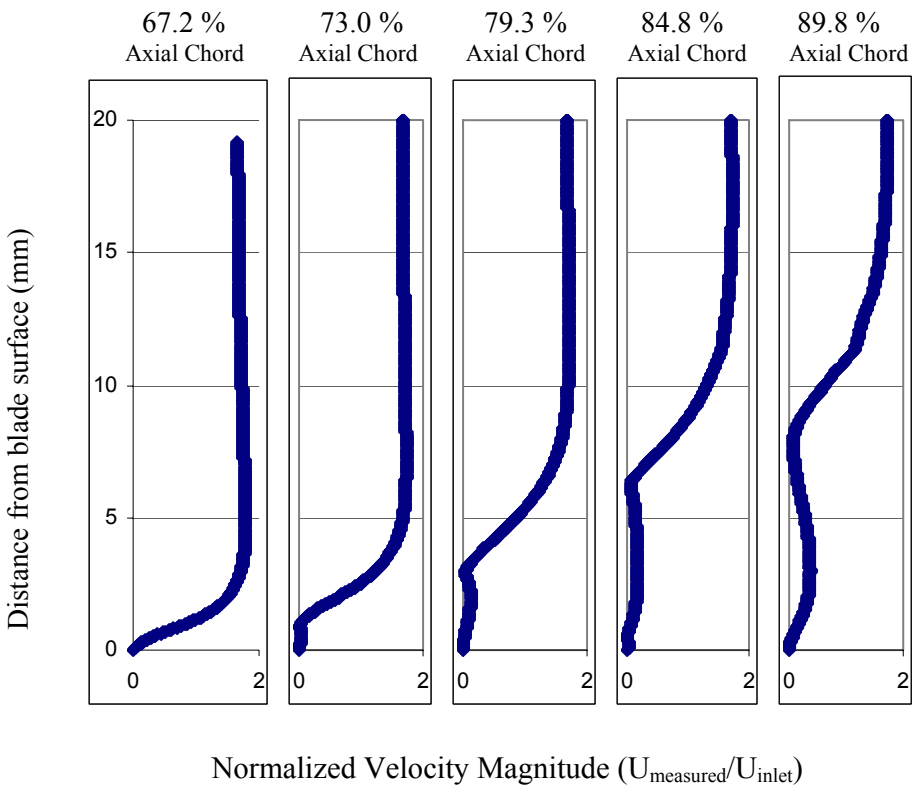

Figure 17: Boundary layer profiles for unmodified Pak-B blade at Re 25k using DES turbulence model at 0.3495 s

For purposes of comparison, Fig. 18 shows boundary layer profiles determined both computationally and experimentally by Casey [4] for an unmodified blade using a laminar solver.

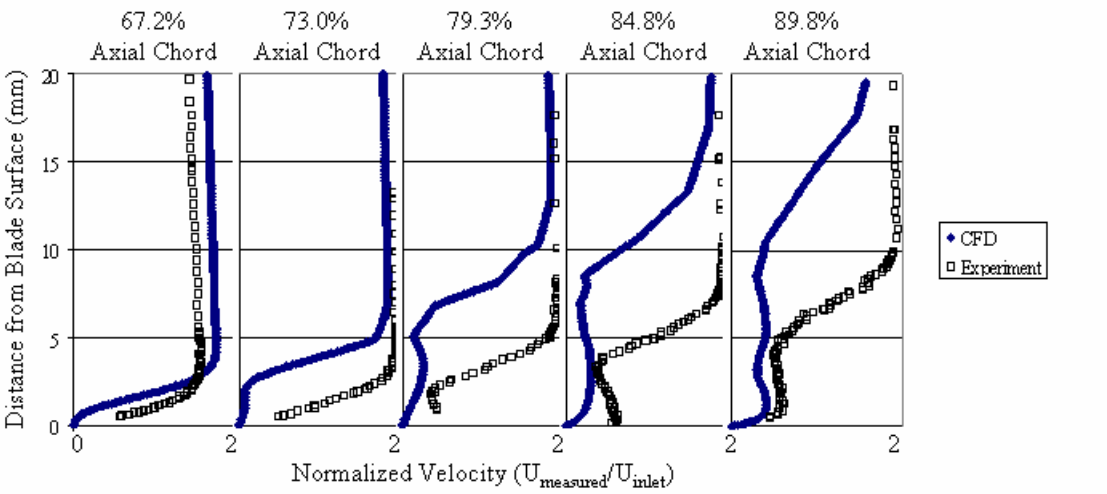

Figure 18: Boundary layer comparisons between laminar CFD model and experiment for an unmodified Pak-B blade at Re 25k and 0% turbulence [Casey,4]

3.4 Summary and Conclusions for Unmodified Blade

According to calculations made by Fieldview®, the flow does not separate to any significant degree until it has reached approximately 90% of axial chord. This result does not match either the velocity magnitude contour plot in Fig. 13 or the boundary layer profiles determined for this research shown in Fig. 17 or determined by Casey [4] in his research shown in Fig. 18. Each of these other data sources indicates that separation begins to occur closer to 65% of axial chord. The difference between this data and these other data sources indicates that the separation location calculated by Fieldview® is incorrect and should be disregarded. As such, it was not possible to determine an exact separation location. However, analysis of the other data sources indicates that separation occurred near the position discovered by Casey [4].

The velocity magnitude contour plot and the associated vector plots provide much more reliable interpretation of the data. According to the contour plot, the flow separates from the blade surface around 65% of axial chord and does not reattach. Also, it shows

that the flow field in the turbulent region is dominated by vortical structures that induce a significant back flow. These results closely match similar results reported by Casey [4]. These images verify that the DES model can resolve turbulent structures in the flow field. This makes sense since the DES model is equivalent to the LES model in any region with significant amounts of turbulence.

The boundary layer profiles are primarily used to determine the thickness of the boundary layer. In this case, the boundary layer significantly increases in thickness as the flow moves downstream. Though these results do not perfectly match Casey's [4] experimental results, they do compare favorably to his computational results, for which he employed a laminar solver. At 67.2% of axial chord, both sets of computational data match each other closely. However, as the flow moves downstream, the results from this research show a smaller boundary layer than the results from Casey's [4] computational research. This lower recorded thickness for the DES model more closely matches the experimentally observed boundary layer thickness recorded by Casey [4]. This represents the first significant advantage of the DES turbulence model over the laminar solver. It should be noted that Casey's [4] results are time-averaged whereas the results from this research are not. However, this difference is not expected to have a great effect on this comparison.

For most of the research data, the DES turbulence model proved either as accurate or more accurate than the laminar solver for an unmodified Pak-B blade. Since Casey [4] already determined that the laminar solver is more accurate than other currently available turbulence models, future researchers should strongly consider using the DES model in their research.

3.4 Results for Pak-B Blade with Dimple at 65% of Axial Chord

3.4.1 Separation Location

Fig. 19 shows a diagram of the locations of separation and reattachment as calculated by Fieldview® at 0.15 s of flow time. The diagram shows that the flow separated from the blade as it enters the dimple and reattaches as it exits the dimple. Subsequently, the flow separates again at approximately 72% of axial chord. Beyond this, there is no significant line of reattachment. For comparison, Casey [4] found the contained vortex within the dimple and calculated the separation line at 71% of axial chord. Subsequently, he discovered that the flow reattaches at 83% of axial chord. Even though the results from this study show separation downstream of Casey's results, Casey also discovered that the separation location moves upstream as the flow time progressed so the results are consistent.

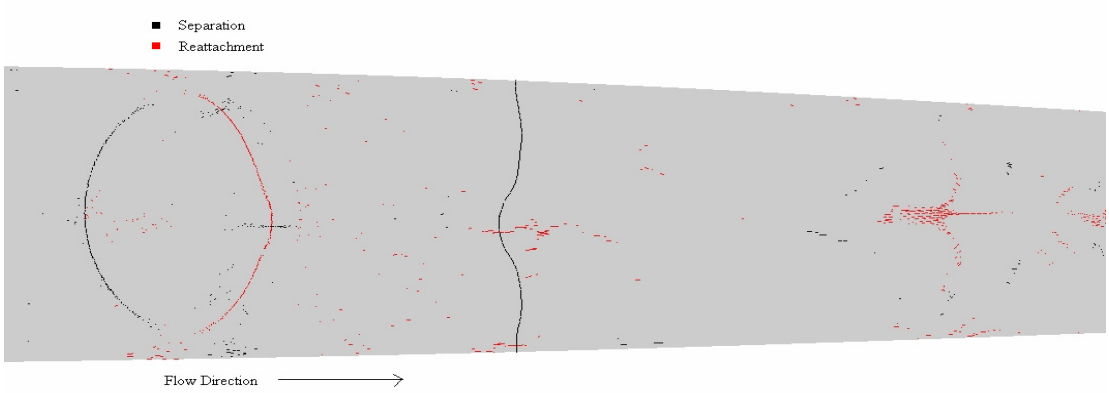

Figure 19: Separation and reattachment lines for Pak-B blade with dimple at 65% of axial chord for Re 25k using DES turbulence model at 0.15 s

3.4.2 Velocity Field Plots

Fig. 20 shows the velocity magnitude contours of the computational flow field for a Pak-B blade with a dimple located at 65% of axial chord on a plane located at the mid-span of the blade. It illustrates the presence of vortical structures within the turbulent

region of the flow field. Also, Fig. 20 shows that the flow separates from the blade surface at the position where the boundary layer begins to move away from the blade. Note that the presence of the dimple causes separation to occur farther downstream than for the unmodified case. Span-wise uniformity of the contour plots were checked and no significant differences were discovered.

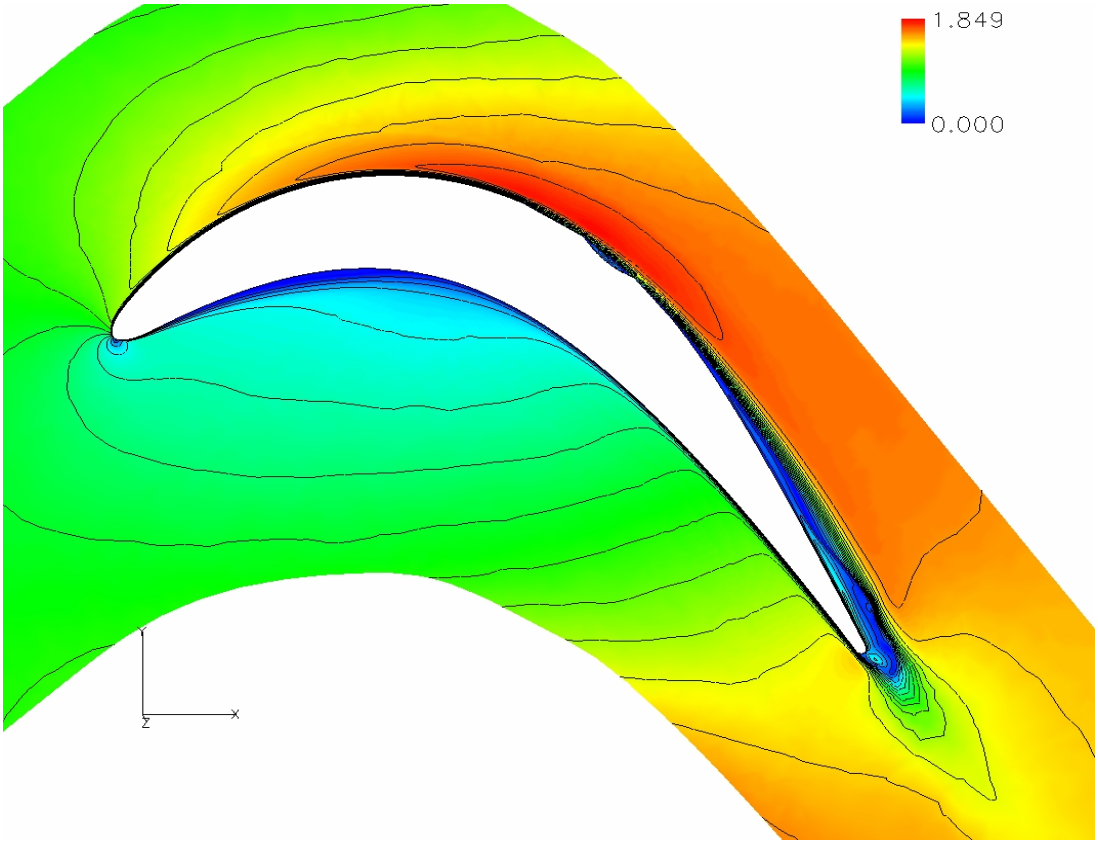

Figure 20: Normalized velocity magnitude contour plot for Pak-B blade with dimple at 65% of axial chord at Re 25k using DES turbulence model at 0.15 s

Fig. 21 shows the vector field for the turbulent region of the dimpled case. Note the presence of vortical structures though the structure is much closer to the trailing edge of the blade than for the unmodified case.

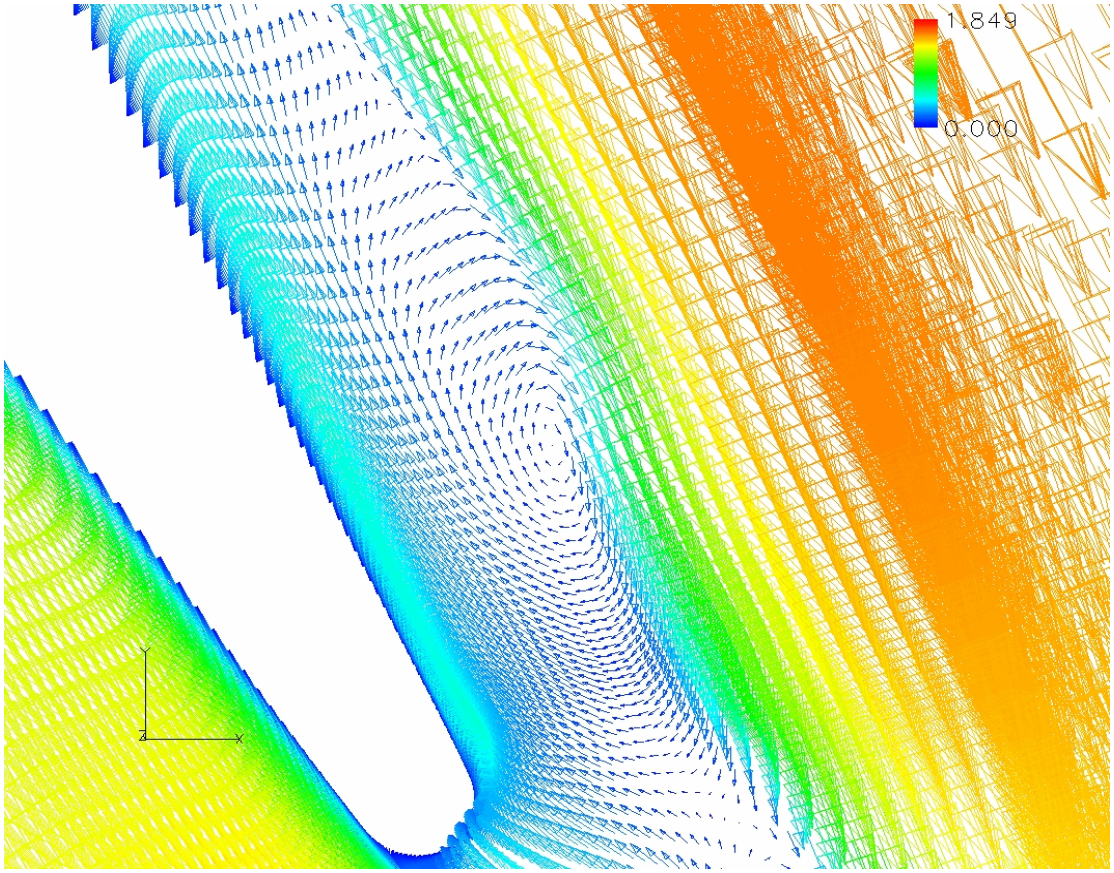

Figure 10: Vector field of velocity magnitude in turbulent region for Pak-B blade with dimple at 65% of axial chord at Re 25k using DES turbulence model at 0.15 s

Fig. 22 shows the vector field of the flow as it enters the dimple. Note that the flow travels uniformly downstream until it enters the dimple at which point it gets caught up in the dimple's contained vortex.

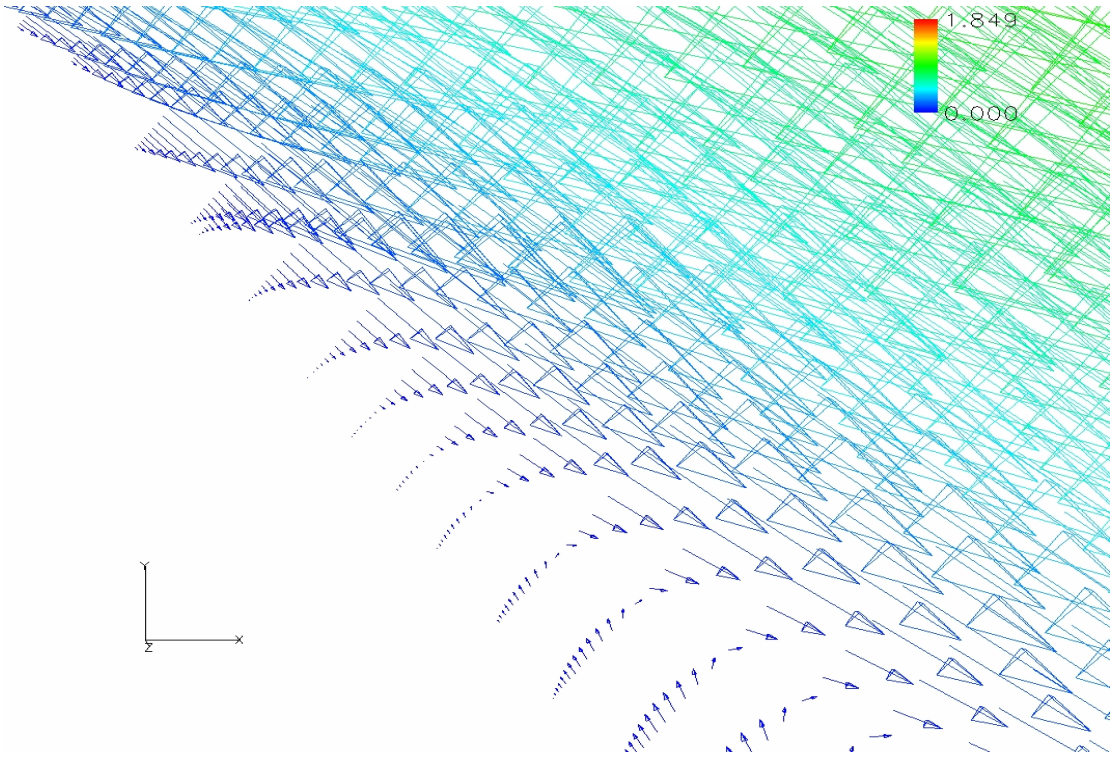

Figure 22: Vector field of velocity magnitude of flow entering dimple for Pak-B blade with dimple at 65% of axial chord at Re 25k using DES turbulence model at 0.15 s

3.4.3 Streamline Visualizations

Fig. 23 displays the behavior of the streamlines of the flow field released from a row of seeds located at 50% of axial chord. The streamline visualization shows that the vortex contained within the dimple captures the streamlines and pulls them into the dimple. Subsequently, the dimple expels the flow down the centerline. It stays at the centerline until it enters the turbulent region of the flow field and the flow becomes very chaotic.

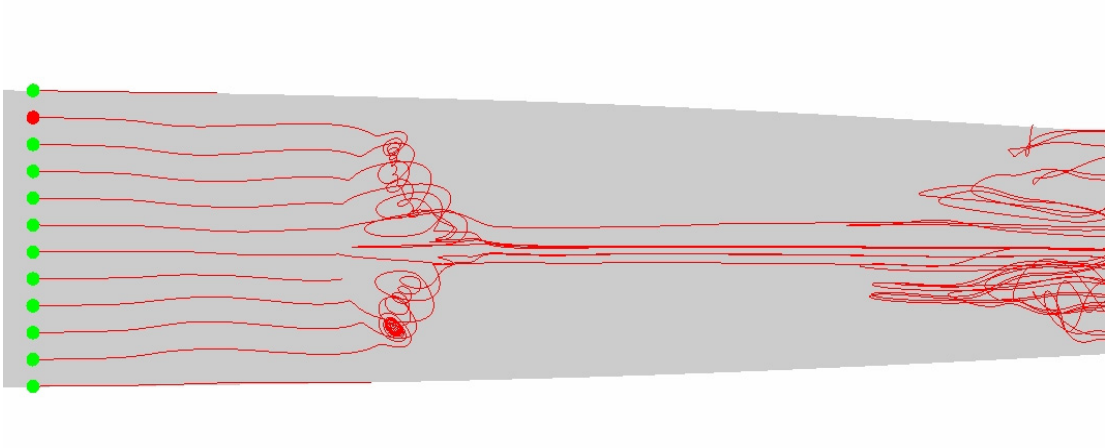

Figure 23: Streamline visualization of flow field for Pak-B blade with dimple at 65% of axial chord at Re 25k using DES turbulence model at 0.15 s

Fig. 24 shows a side view of the streamlines within the dimple. The streamlines clearly show the contained vortex within the dimple.

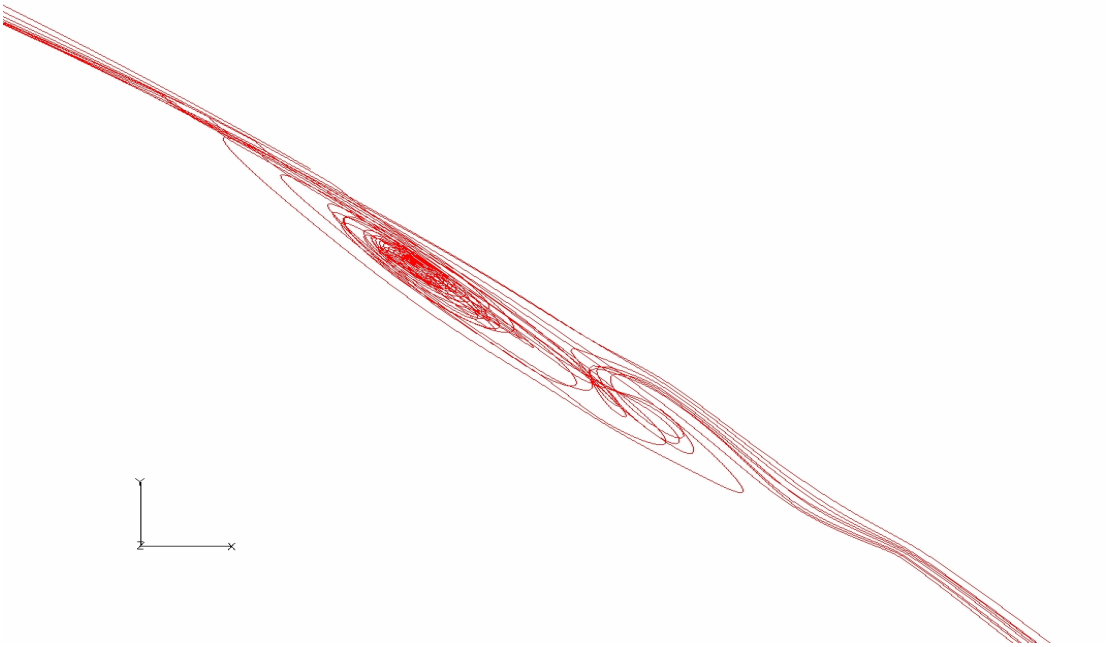

Figure 24: Streamline visualization of dimple within flow field of Pak-B blade with dimple at 65% of axial chord at Re 25k using DES turbulence model at 0.15 s

3.4.4 Boundary Layer Profiles

Fig. 25 shows profiles of the boundary layer constructed for the Pak-B computational model with a dimple located at 65% of axial chord along the mid-span of the blade. At 67.2% and 73.0% of axial chord, there is little evidence of separation. By 79.3% of axial chord, there is a small separation bubble. As the flow moves downstream, the separation bubble steadily grows in size.

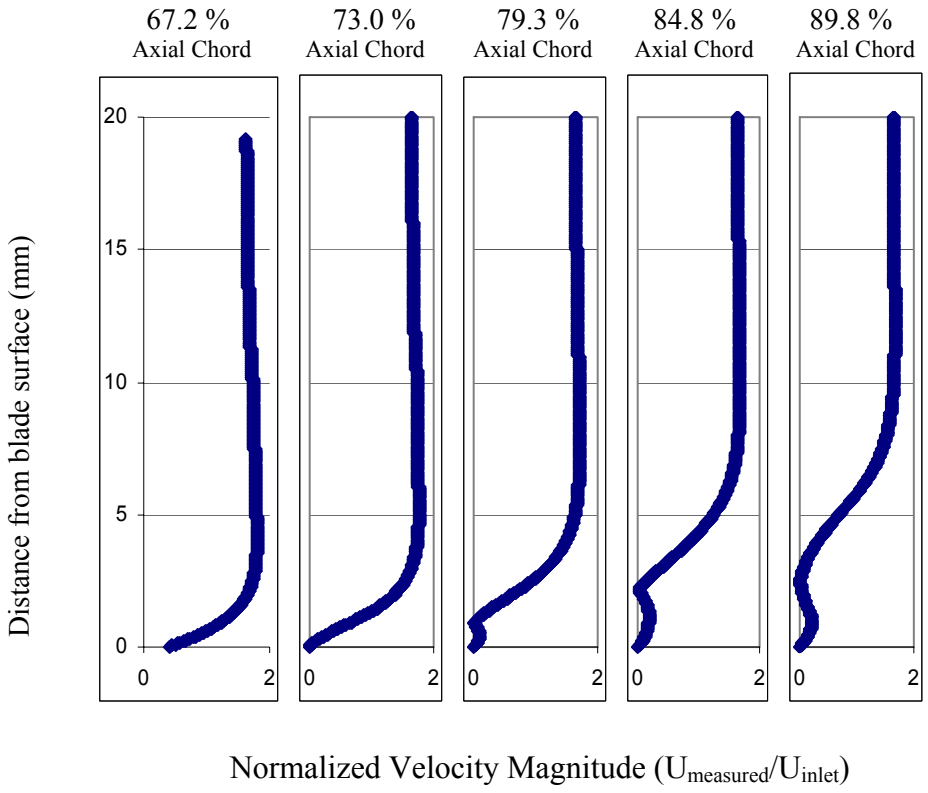

Figure 25: Boundary layer profiles for Pak-B blade with dimple at 65% of axial chord at Re 25k using DES turbulence model at 0.15 s

For purposes of comparison, Fig. 26 shows Casey's experimental and computational results for this case.

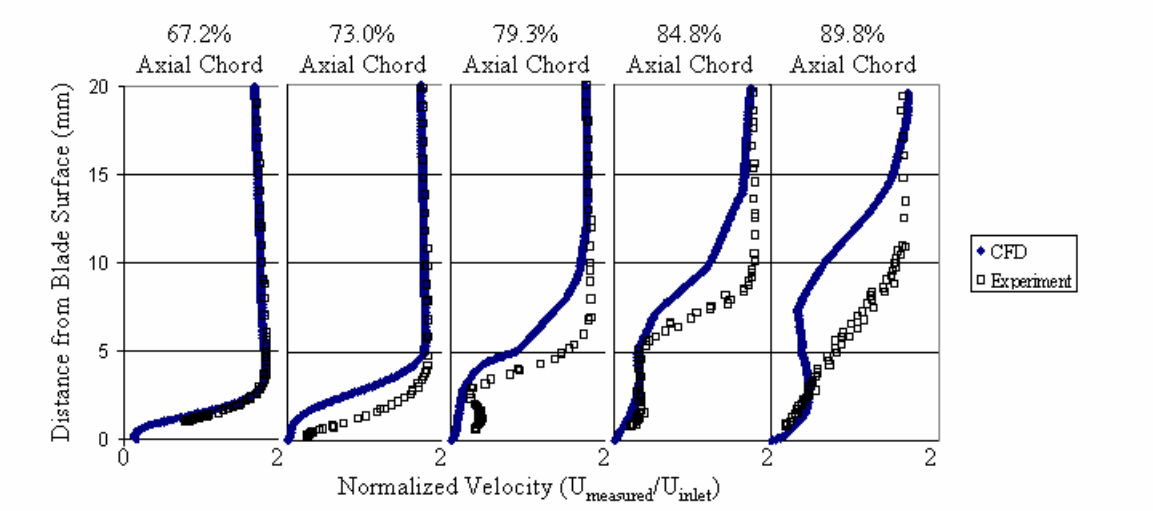

Figure 26: Boundary layer comparisons between CFD and experiment for a Pak-B blade with dimple at 65% of axial chord at Re 25k and 1% Tu [Casey,4]

3.5 Summary and Conclusions for Pak-B Blade with Dimple at 65% of Axial Chord

According to calculations made by Fieldview®, the flow separates around 73% of axial chord. This result matches other data sources such as the velocity magnitude plots and boundary layer profiles. This differs from the results for the unmodified blade. This difference may result from the major differences in the respective flow fields. For this case, the dimple works to change the flow field from laminar to turbulent. However, with the unmodified blade, there is no structure designed to accomplish this so the solver must decide where the flow transitions. On the other hand, these results do not show the subsequent reattachment discovered both experimentally and computationally by Casey [4]. However, since the flow field did not develop as greatly for this research, it is possible that further development would show reattachment.

According to the contour plot, the flow separates from the blade surface well downstream of the dimple. Also, it shows that the flow field in the turbulent region is

marked by vortical structures that induce a significant back flow. However, these results do not show as much turbulent activity in the form of localized regions of high velocity as reported by Casey [4] in his computational results. Again, this difference may result from the fact that Casey [4] was able to develop the flow field to a greater extent than reached in this research. These images also verify that the DES model can resolve turbulent structures in the flow field. This makes sense since the DES model is equivalent to the LES model in any region with significant amounts of turbulence.

The streamlines show the same behavior as reported by Casey [4] in his research. Specifically, they show that the dimple vortex captures the streamlines and pulls them into the dimple and expels them along the centerline of the dimple.

The boundary layer profiles are primarily used to determine the thickness of the boundary layer. In this case, the boundary layer increases in thickness as the flow moves downstream. Though these results do not perfectly match Casey's [4] experimental results, they do compare favorably to his computational results, for which he employed a laminar solver. At 67.2% of axial chord, both sets of computational data match each other closely. At 73.0% of axial chord, Casey's [4] computational data shows a small separation bubble whereas neither his computational data nor the data from this research shows this feature. As the flow moves downstream, the results from this research match Casey's [4] experimental research better than the results from Casey's [4] computational research. It should be noted that Casey's [4] results are time-averaged whereas the results from this research are not. However, this difference is not expected to have a great effect on this comparison.

For most of the research data, the DES turbulence model proved either as accurate or more accurate than the laminar solver for a Pak-B blade with a dimple located at 65% of axial chord. These results strengthen the contention that future researcher should strongly consider the DES turbulence model.

Chapter 4: Summary and Recommendations

As flight technology has advanced, the United States military has begun to rely more heavily on unmanned aerial vehicles, such as the Navy's X-47 Pegasus, to complete essential missions. These aircraft often fly at high altitudes and low speeds, conditions that lead to low Reynolds numbers. Ultimately, these conditions cause flow separation off the blades of low pressure turbines and thereby greatly decrease the effectiveness of the aircraft so that variables such as range and endurance are decreased.

Given these difficulties, many resources have been invested into research of both active and passive separation control methods. Advantageously, passive controls help to conserve the aircraft's energy and are particularly useful in systems in which flow conditions maintain fairly steady values. Researchers have shown that dimples are among the more successful passive control devices. Specifically, spherical dimples placed at 65% of axial chord have proven to optimize the loss reduction for LPT blades.

Unfortunately, the CFD research has lagged behind the experimental research. To date, no turbulence model exists that can accurately resolve the entire flow field. Previously, a laminar viscous model had been most successful at solving this problem. The current research aimed to investigate the effectiveness of the detached eddy simulation turbulence model. Two cases were studied using this model: an unmodified Pak-B blade and a Pak-B blade with a spherical dimple located at 65% of axial chord. The DES model was used to determine the separation location, prepare velocity magnitude contour plots and vector plots of the flow field, visualize the streamlines associated with the dimple, and create boundary layer profiles from which the thickness

of the boundary layer could be determined. Overall, the DES turbulence model outperformed the laminar solver.

Regarding the use of the DES model to analyze dimples on low pressure turbine blades, more research remains to be done. To ensure that the CFD solutions are as physically accurate as possible, rigorous grid- and time-independence studies should be performed. Also, a study should be performed to either assure that the default values for the turbulence model optimize its accuracy or, if not, determine what values would do so. Also, future research should endeavor to extend the amount of flow time for which a solution is obtained.

In conclusion, this research provided information regarding the ability of the DES turbulence model to accurately resolve the flow field for both an unmodified Pak-B blade and a similar blade with a dimple. In many respects, the DES model proved to be as successful as any other solver for these cases. This will benefit researchers since they can now more reliably predict experimental results using CFD simulations.

Appendix A: Sample Computer Files

Example of Fluent® infile used in research; called from batch submission script:

```
file
rcd
<file name of file that Fluent® should call>
q
q
file
read-macros
macros.scm
q
q
grid
reorder
reorder-domain
q
q
q
define
models
unsteady-2nd-order
q
q
solve
set
time-step
0.00005
q
dual-time-iterate
2000
20
q
q
file
wcd
<file name that Fluent® should write to>
q
q
/parallel/timer/print
q
q
exit
y
```

Example of batch submission script used in research:

```
#!/bin/csh -x
#BSUB –J <job name>
#BSUB –n <number of processors>
#BSUB –W <maximum clock time desired in hh:mm format>
#BSUB –q Default
#BSUB –o <output file>
#BSUB –e <error file>
#BSUB –P <16 character account number>

cd $WORK_DIR

/usr/bin/rcp <case file path> .
/usr/bin/rcp <data file path> .
/usr/bin/rcp <infile path> .

fluent 3ddp –g –ptmpi –t <number of processors> -i <infile name> >& new.out

/usr/bin/rcp <output case file name> ${msas}:<case file path> .
/usr/bin/rcp <output data file name> ${msas}:<data file path> .
/usr/bin/rcp <out file name> ${msas}:<data file path> .
```

Example of macro file used in research to periodically write Fieldview® files; called from Fluent® infile:

```
(cx-macro-define
 '((fv . "\nfile\nexport\nfieldview\n<file name%t>\npressure\ndyn\ntotal\nx-vel\ny-vel\nz-vel\nq\n")
  ))
```

References

1. Rouser, Kurt P. *Use of Dimples to Suppress Boundary Layer Separation on a Low Pressure Turbine Blade*. MS Thesis, AFIT/GAE/ENY/02-13. Graduate School of Engineering and Management, Air Force Institute of Technology (AU), Wright-Patterson AFB, OH, 2002 (ADA409462)
2. Northrup Grumman Capitol Source. *Naval Unmanned Combat Aerial Vehicle*, (09 August 2002). 1 June 2004 http://www.capitol.northgrum.com/programs/pegasus.html.
3. Lake, James P. *Flow Separation Prevention on a Turbine Blade in Cascade at Low Reynolds Numbers*. PhD Dissertation, AFIT/DS/ENY/99-01. Graduate School of Engineering and Management, Air Force Institute of Technology (AU), Wright-Patterson AFB, OH, 1999
4. Casey, John P. *Effect of Dimple Pattern on the Suppression of Boundary Layer Separation on a Low Pressure Turbine Blade*. MS Thesis, AFIT/GAE/ENY/04-M05. Graduate School of Engineering and Management, Air Force Institute of Technology (AU), Wright-Patterson AFB, OH, 2004.
5. Sharma, O. "Impact of Reynolds Number on LP Turbine Performance," *Proceedings of the 1997 Minnowbrook II Workshop on Boundary Layer Transition in Turbomachines*. 65-59. NASA CP-1998-206958, 1998.
6. Murawski, C.G., R. Sondergaard, R.B. Rivir, T.W. Simon, K. Vafai, and R.J. Volino. "Experimental Study of the Unsteady Aerodynamics in a Linear Cascade with Low Reynolds Number Low Pressure Turbine Blades," *International Gas Turbine Institute and Aeroengine Congress and Exposition*. ASME Paper 97-GT-95. Orlando, FL, June 1997.
7. Qiu, S. and T.W. Simon. "An Experimental Investigation of Transition as Applied to Low Pressure Turbine Suction Surface Flows," *International Gas Turbine Institute and Aeroengine Congress and Exposition*. ASME Paper 97-GT-455. Orlando, FL, June 1997.
8. Simon, T.W. and R.J. Volino. "Separating and Separated Boundary Layers," Technical Report WL-TR-96-2092, Wright Laboratory, 1996.
9. Mattingly, J.D. *Elements of Gas Turbine Propulsion*. New York: McGraw-Hill, 1996.
10. Oates, Gordon C. *Aerothermodynamics of Gas Turbine and Rocket Propulsion* (Third Edition). Reston, VA: American Institute of Aeronautics and Astronautics, 1997.
11. Moran, Michael J. and Howard N. Shapiro. *Fundamentals of Engineering Thermodynamics* (4th Edition). New York: John Wiley & Sons, 2000.
12. Anderson, John D. *Modern Compressible Flow with Historical Perspective* (Third Edition). New York: McGraw-Hill, 2003.

13. Halstead, D.E., D.C. Wisler, T.H. Okiishi, G.J. Walker, and H.P. Hodson. "Boundary Layer Development in Axial Compressors and Turbines – Part 1 of 4: Computations and Analysis," *International Gas Turbine Institute and Aeroengines Congress and Exposition*. ASME Paper 95-GT-461. Houston, TX, June 1995.

14. Halstead, D.E., D.C. Wisler, T.H. Okiishi, G.J. Walker, and H.P. Hodson. "Boundary Layer Development in Axial Compressors and Turbines – Part 3 of 4: LP Turbines," *International Gas Turbine Institute and Aeroengines Congress and Exposition*. ASME Paper 95-GT-463. Houston, TX, June 1995.

15. Mayle, R.E. "The Role of Laminar-Turbulent Transition in Gas Turbine Engines," *Journal of Turbomachinery*, 113:509-537 (October 1991).

16. Addison, J.S. and H.P. Hodson. "Modeling of Unsteady Transition Boundary Layers," *International Gas Turbine Institute and Aeroengines Congress and Exposition*. ASME Paper 91-GT-282. Orlando, FL, June 1991.

17. Walker, G.J. "The Role of Laminar-Turbulent Transition in Gas Turbine Engines: A Discussion," *Journal of Turbomachinery*, 115:207-217 (April 1993).

18. Werle, M.J. "Compressor and Turbine Blade Boundary Layer Separation," *AGARD Conference Proceedings*, AGARD-CP-351 (1983).

19. Halstead, D.E., D.C. Wisler, T.H. Okiishi, G.J. Walker, and H.P. Hodson. "Boundary Layer Development in Axial Compressors and Turbines – Part 3 of 4: Composite Picture," *International Gas Turbine Institute and Aeroengines Congress and Exposition*. ASME Paper 95-GT-464. Houston, TX, June 1995.

20. Rizzeta, D.P. and M.R. Visbal. "Numerical Investigation of Transitional Flow Through a Low-Pressure Turbine." Power Point presentation to Dayton-Cincinnati Aerospace Science Symposium. 9 March 2004.

21. Prasad, R., A. Bakker, and L. Marshall. "Numerical Modeling of Mixing Processes – What Can LES Offer?" Power Point presentation. 20 May 2004 www.bakker.org/cfm/lesaiche98.pdf.

22. Kapadia, S., S. Roy, and K. Wurtzler. "Detached Eddy Simulation Over a Reference Ahmed Car Model," *41st Aerospace Sciences Meeting and Exhibit*. AIAA Paper 2003-0857. Reno, NV, 6-9 January 2003. 20 May 2004 cpdl.kettering.edu/AIAA-2003-0857.pdf.

23. Spalart, P.R. "Young Person's Guide to Detached-Eddy Simulation Grids," NASA/CR-2001-211032, July 2001. 22 March 2004 techreports.larc.nasa.gov/ltrs/PDF/2001/cr/NASA-2001-cr211032.pdf.

24. Johnston, J.P. and M. Nishi. "Vortex-generator Jets-Means for Separation Flow Control," *AIAA Journal*, Vol. 28, No. 6, 989-994 (June 1990).

25. Compton, D.A. and J.P. Johnston. "Streamwise Vortex Production by Pitched and Skewed Jets in a Turbulent Boundary-Layer," *AIAA Journal*, Vol. 30, No. 3, 640-647 (March 1992).

26. Bons, J.P., R. Sondergaard, and R. Rivir. "Turbine Separation Control Using Pulsed Vortex Generator Jets," *ASME Journal*, Vol. 123, 198-206 (April 2001).

27. Borgeson, David. *Boundary Layer Control Using Micro-Electromechanical Systems*. MS Thesis. AFIT/GSO/ENP/02-1. Graduate School of Engineering and Management, Air Force Institute of Technology (AU), Wright-Patterson AFB, OH, 2002 (ADA 401590)

28. Lin, J.C., F.G. Howard, D.M. Bushnell, and G.V. Shelby. "Investigation of Several Passive and Active Methods of Turbulent Boundary Layer Control," AIAA Paper 90-598, 1990.

29. Austin, J.G. *Mach Number, Flow Angle, and Loss Measurements Downstream of a Transonic Fan-Blade Cascade*. MS Thesis. Naval Postgraduate School, Monterey, CA, March 1994 (ADA280907).

30. Gamerdinger, P.M. and R.P. Shreeve. "The Effects of Low-Profile Vortex Generators on Flow in a Transonic Fan-Blade Cascade," *34th Aerospace Sciences Meeting and Exhibit*. AIAA Paper 96-0250. Reno, NV, January 1996.

31. Rao, D.M. and T.T. Kariya. "Boundary-Layer Submerged Vortex Generators for Separation Control – An Exploratory Study," *1st National Fluid Dynamics Congress, 1988*. AIAA Paper 88-3546-CP.

32. Lin, J.C., F.G. Howard, and G.V. Shelby. "Turbulent Flow Separation Control Through Passive Techniques," *AIAA 2nd Shear Flow Conference*. AIAA Paper 89-0976. Tempe, AZ, March 1989.

33. McCormick, D.C. "Shock-Boundary Layer Interaction Control with Low-Profile Vortex Generators and Passive Cavity," *30th Aerospace Sciences Meeting and Exhibit*. AIAA Paper 92-0064. Reno, NV, January 1992.

34. Bloch, D.R. and T.J. Mueller. "Effects of Distributed Grit Roughness on Separation and Transition on an Airfoil at Low Reynolds Numbers," AIAA Paper 86-1788. 1988.

35. Taylor, H.D. *Summary Report on Vortex Generators*. Technical Report R-052080-9. United Aircraft Corporation Research Department, March 1950.

36. Bearman, P.W. and J.K. Harvey. "Control of Circular Cylinder Flow by the Use of Dimples," *AIAA Journal*, Vol. 31, No. 10, 1753-1756 (October 1993).

Vita

Ensign Kyle P. Malone graduated from Academy of Holy Angels High School in Richfield, Minnesota. He entered undergraduate studies at Marquette University in Milwaukee, Wisconsin where he graduated with a Bachelor of Science degree in Mechanical Engineering in May 2003. He was commissioned through the NROTC unit at Marquette University.

Upon commissioning, he reported for his first assignment as a student in the Graduate School of Education and Management at the Air Force Institute of Technology on Wright-Patterson AFB in Dayton, Ohio to pursue graduate studies in aeronautical engineering. At AFIT, he was inducted into Tau Beta Pi. Upon graduation, he will attend flight school at NAS Pensacola in Pensacola, Florida.

REPORT DOCUMENTATION PAGE

Form Approved
OMB No. 074-0188

1. REPORT DATE *(DD-MM-YYYY)*	**2. REPORT TYPE**	**3. DATES COVERED** *(From – To)*
15-06-2004	Master's Thesis	June 2003-June 2004

4. TITLE AND SUBTITLE

DETACHED EDDY SIMULATION ANALYSIS OF PAK-B LOW PRESSURE TURBINE BLADE

5a. CONTRACT NUMBER

5b. GRANT NUMBER

5c. PROGRAM ELEMENT NUMBER

6. AUTHOR(S)

Malone, Kyle, P., Ensign, USNR

5d. PROJECT NUMBER

5e. TASK NUMBER

5f. WORK UNIT NUMBER

7. PERFORMING ORGANIZATION NAMES(S) AND ADDRESS(S)
Air Force Institute of Technology
Graduate School of Engineering and Management (AFIT/EN)
2950 Hobson Way
WPAFB OH 45433-7765

8. PERFORMING ORGANIZATION REPORT NUMBER

AFIT/GAE/ENY/04J-06

9. SPONSORING/MONITORING AGENCY NAME(S) AND ADDRESS(ES)
AFRL/PRTT
Attn: Dr. Rolf Sondergaard
1950 5th Street
WPAFB OH 45433-7251 DSN: 785-7190

10. SPONSOR/MONITOR'S ACRONYM(S)

11. SPONSOR/MONITOR'S REPORT NUMBER(S)

12. DISTRIBUTION/AVAILABILITY STATEMENT
APPROVED FOR PUBLIC RELEASE; DISTRIBUTION UNLIMITED.

13. SUPPLEMENTARY NOTES

14. ABSTRACT

Two cases were computationally investigated using the detached eddy simulation (DES) turbulence model: an unmodified Pak-B blade and a Pak-B blade with a dimple located at 65% of axial chord. Both cases were created so that they simulated an infinite span with an infinite number of dimples. The cases were run for an inlet Reynolds number of 25,000. The computed results were used to resolve the location of separation and reattachment, visualize the streamlines for the dimpled case, build velocity magnitude contour and vector plots, and map the thickness of the boundary layer. The results were then compared to previous computational and experimental studies in order to validate the detached eddy simulation model for future research into the effect of dimples on low pressure turbine flow fields. For the unmodified blade, the performance of the DES model compared favorably to other available viscous and turbulence models. For the dimpled blade, preliminary results also compare favorably to other models although further development of the flow field is needed to verify this. Based on these results, future researchers studying dimples on turbine blades should strongly consider using the DES turbulence model.

15. SUBJECT TERMS
Laminar Boundary Layer Separation, Boundary Layer Transition, Turbulent Boundary Layer, Boundary Layer Trips, Passive Boundary Layer Controls, Passive Flow Controls, Low Pressure Turbine Blade, Low Pressure Turbine Blade Performance, Gas Turbine Engine, Low Reynolds Number, Computational Fluid Dynamics, CFD, Boundary Layer Measurements, DES, Detached Eddy Simulation

16. SECURITY CLASSIFICATION OF:			**17. LIMITATION OF ABSTRACT**	**18. NUMBER OF PAGES**	**19a. NAME OF RESPONSIBLE PERSON**
REPORT	**ABSTRACT**	**c. THIS PAGE**			Dr. Paul I. King (ENY)
U	**U**	**U**	**UU**	71	**19b. TELEPHONE NUMBER** *(Include area code)* (937) 255-6565, ext 4314; e-mail: Paul.King@afit.edu